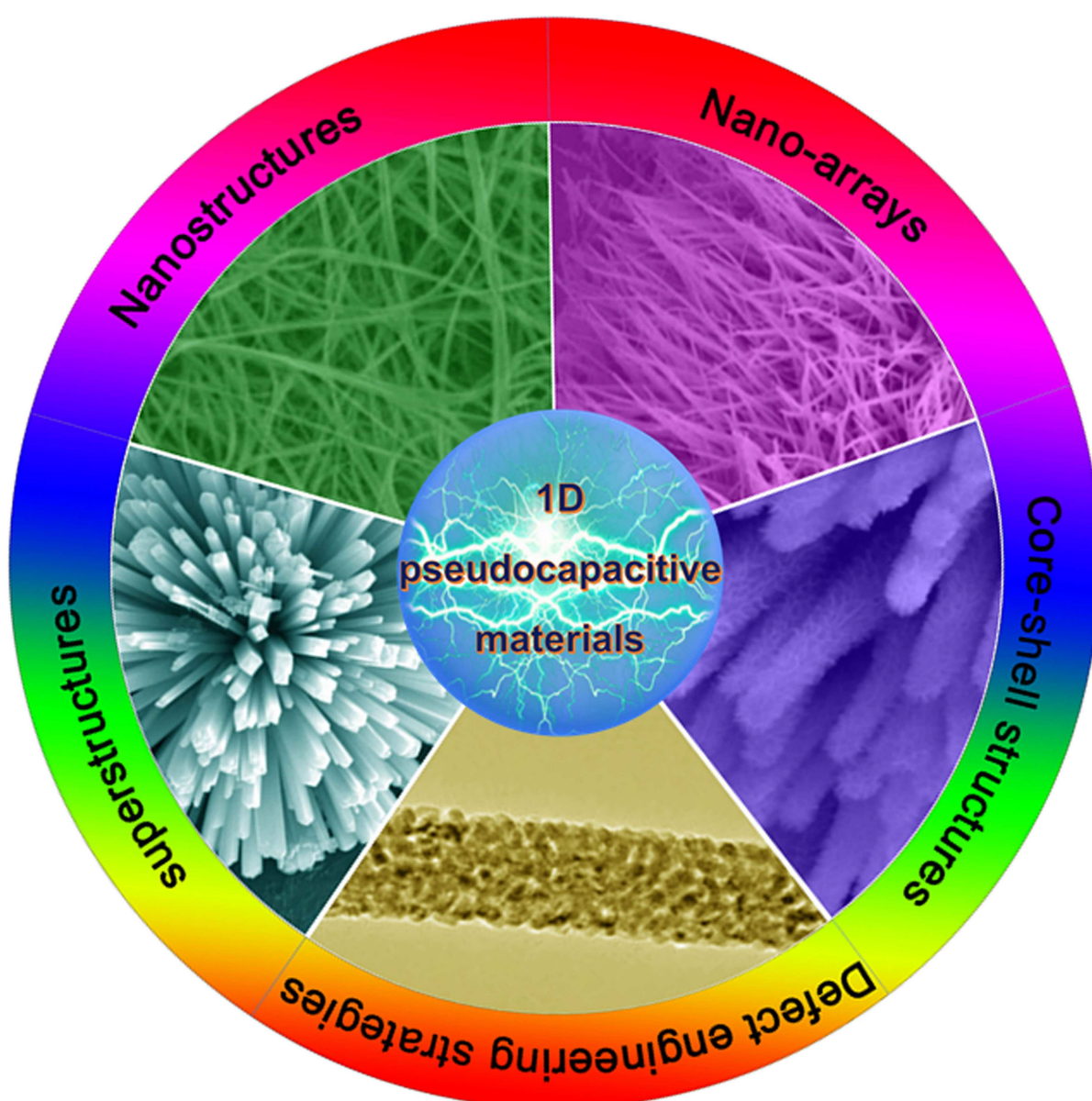


One-Dimensional Nanostructured Pseudocapacitive Materials: Design, Synthesis and Applications in Supercapacitors

Jinfeng Sun,^[a] Lingzhi Guo,^[a] Xuan Sun,^[a] Jinyang Zhang,^[a] Linrui Hou,^[a] Li Li,^[a] Shuhua Yang,^[a] and Changzhou Yuan^{*[a]}



In the past decades, pseudocapacitive materials (PCMs) for electrochemical energy storage have drawn enthusiastic attention from researchers, owing to their virtue of larger Faradaic capacitance facilitating enhanced energy densities compared to electric double-layer capacitive materials. To maximize capacitive properties without sacrificing power densities, novel design and fine fabrication of innovative PCMs with rational microstructures become of significant importance. Typically, enormous efforts have been devoted to fabricating 1D nanostructured PCMs for advanced supercapacitors, thanks to their geometrical merits facilitating the ionic/electronic transport. This review mainly focuses on the latest development and progress of 1D nanostructured PCMs for advanced super-

capacitors. Firstly, typical pseudocapacitive mechanisms are discussed in detail. Secondly, physicochemical properties and intrinsic merits of 1D nanoscaled electrodes are comprehensively described. Thirdly, representative synthetic methodologies, optimization strategies and involved formation mechanisms for 1D nanodimensional PCMs are surveyed. Besides, the applications of 1D versatile PCMs including 1D conventional nanostructures, nano-arrays, core-shell nano-architectures and secondary superstructures are systematically summarized as competitive electrodes for supercapacitors. Finally, future challenges, prospects and opportunities of 1D nanostructured PCMs for next-generation supercapacitors are further proposed.

Introduction

During the past decades, supercapacitors have been going through a rapidly development. Supercapacitors have been considered as one of the most promising electrochemical energy storage systems in view of their outstanding features including high power density, fast charge-discharge performance, and ultra-long cycle life ($> 10^5$ cycles).^[1–3] However, supercapacitors often suffer from much lower energy density ($\sim 5\text{--}10 \text{ Wh kg}^{-1}$) than secondary batteries ($\sim 200 \text{ Wh kg}^{-1}$), which has been considered as the major issue for expanding their commercial market.^[4] It is an ongoing research priorities that how to hugely improve the energy storage capability of supercapacitors without sacrificing their power density meanwhile. According to the formula: $E = V \int_{V_2}^{V_1} CdV$ where E , C and V are the energy density, specific capacitance (SC) and working potential of the devices, respectively. There are two general approaches to improve the energy storage capability. One is broadening the operating voltage window of the full cell, including asymmetric designing and new electrolytes,^[5–7] and the other is to improve the capacitance of the device. One especially notes that both of the two approaches require the noteworthy development of proper electrode materials.

As for those electrodes with surface Faradic redox reactions involved pseudocapacitive behaviors, their SCs are always even higher than those of electrical double-layer capacitances (EDLCs).^[8–10] Thus, conventional pseudocapacitive materials (PCMs), such as transition metal oxides/chalcogenides/nitrides/selenides (e.g., RuO_2 , MnO_2 , MoS_2 , VN , etc.) and conducting polymers (CPs) including polyaniline (PANI), polypyrrole (PPy), polythiophene (PT) and their derivatives for supercapacitors have obtained enthusiastic attentions.^[11–16] However, there are still some drawbacks that hinder enormous development of the PCMs, including the unsatisfactory rate capability and poor

cycling performance, which are associated to the pseudocapacitance-related huge volume change during the charge-discharge process.^[17] If electrochemical energy storage performance of the PCMs was further purposefully optimized, novel design of electrode architectures would become crucially significant and urgent.^[18] Owing to the rapid prosperity of nanotechnologies, various nanostructured materials with small size, high surface area, and enhanced kinetics pave the express way for next-generation electrode materials, especially for PCMs.^[18,19]

Among these distinct nano-architectures, one-dimensional (1D) nanostructured PCMs have attracted extensive attentions with an consideration of their unique structural and intrinsic properties.^[20,21] 1D nanostructured PCMs in the forms of nanowires (NWs), nanorods (NRs), nanotubes (NTs), nanobelts (NBs), nanofibers (NFs), etc. can shorten the carrier transportation path, thus enhancing the carrier transport in high charge-discharge rate and enlarging the sur-/interfaces between the electrode and electrolyte meanwhile.^[22–26] It is greatly critical to achieve the high-energy-density supercapacitors but not sacrifice their power behaviors. In the case, researchers made enormous efforts in structural/compositional optimization of 1D PCMs. Thus, 1D nano-arrays, hetero core-shell architectures, 1D nano-blocks-constructed secondary superstructures, and defect engineering 1D PCMs also have been extensively studied.^[27–30] Previous reviews mostly focused on the 1D nanostructured materials and their applications in the field of energy conversion and storage, providing great insights to the energy-related researches.^[31–35]

In the review, we mainly focus on the latest development and structure optimization strategies of 1D nanostructured PCMs for advanced supercapacitors. We first discuss the typical pseudocapacitive mechanisms and provide some new insights on 1D nanostructured PCMs in detail. And then, the physicochemical properties and innate merits of 1D nanoscaled electrodes are demonstrated. Representative synthetic strategies and involved formation mechanisms for 1D nanostructured PCMs are involved in Section 4. Besides, the applications of 1D nanostructured materials are systematically discussed as competitive electrodes for supercapacitors. As shown in Figure 1, the designed versatile structures and optimization

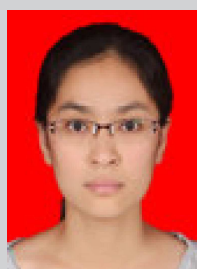
[a] Dr. J. Sun, L. Guo, Dr. X. Sun, Dr. J. Zhang, Prof. L. Hou, Dr. L. Li, Prof. S. Yang, Prof. C. Yuan
School of Materials Science & Engineering
University of Jinan
Jinan, 250022, P. R. China
E-mail: mse_yuan@ujn.edu.cn
ayuan@163.com

strategies, such as NWs/NTs/NRs, nano-arrays, core-shell architectures, secondary superstructures, and defect engineering 1D PCMs are depicted in detail. Finally, future challenges and opportunities of 1D nanostructured PCMs for supercapacitors are also prospectively put forward.

Pseudocapacitive Mechanisms

Since the state-of-the-art RuO₂, involving the Faradaic process with much larger capacitances than EDLCs, was discovered to display pseudocapacitive behaviors, researchers rendered a

new approach to improve the charge storage capacity of the supercapacitors.^[36,37] After that, various pseudocapacitive electrodes have been reported and pseudocapacitive mechanisms have been undergoing uninterrupted exploration, and new insights are further derived.^[38,39] Compared to EDLCs, the Faradaic process is always associated with a valence state change of electroactive materials as a result of the electron transfer.^[4,40] Based on previous distinguished researches, the Faradaic mechanisms are classically identified as the following three categories: (i) underpotential deposition, (ii) redox pseudocapacitance, and (iii) intercalation pseudocapacitance, as schematically illustrated in Figure 2.^[3]



Jinfeng Sun received her Ph.D. degree from Lanzhou Institute of Chemical physics, Chinese Academy of Science in 2015. Then she went to Hong Kong Polytechnic University as a Research Assistant, followed by a post-doctoral fellow. She jointed University of Jinan in 2017. Her research focuses on nanomaterials for supercapacitors and wearable electronics.



Lingzhi Guo received her bachelor's degree from University of Jinan in 2017. She is currently pursuing her master's degree in School of Materials Science & Engineering at University of Jinan. Her research mainly focuses on the design and synthesis of functional materials for advanced energy storage systems.



Xuan Sun received the M. S. in 2014 and B. S. degrees in 2017 from University of Jinan, respectively. She again joined in University of Jinan in 2017, where she works as a Ph. D. candidate at School of Materials Science & Engineering. Her research focuses on the synthesis and characterization of MXene-based materials for energy storage applications (Li-ion and Na-ion batteries).



Jinyang Zhang is currently a PhD candidate under the guidance of Prof. Chang-Zhou Yuan at the University of Jinan. Her research interests focus on the synthesis and applications of metal nanoparticles incorporated into metal-organic frameworks.



Linrui Hou obtained her PhD degree in Industrial Catalysis from Nanjing Tech University, China in 2010. She works now as a full professor at the School of Materials Science and Engineering in University of Jinan. Her current research interests conclude three major frontiers, namely lithium-ion batteries, quantum dots, and photocatalysis.



Li Li is currently a research scientist at University of Jinan. She received her PhD degree from Nankai University in 2014. Her research focuses on the design and synthesis of nano/micromaterials and their applications in Li/Na ion batteries and supercapacitors.



Shuhua Yang received his Ph.D. degree in Materials Science and Engineering from Shanghai Jiao Tong University (SJTU) in 2015. He is now an assistant professor in the School of Material Science and Engineering at University of Jinan. His research focuses on the design and synthesis of functional materials and exploration of their potential application in supercapacitors.



Changzhou Yuan received a PhD from Nanjing University of Aeronautics and Astronautics in 2009. He is a distinguished professor of Taishan Scholar in School of Materials Science and Engineering, University of Jinan. He is Highly Cited Researcher (in Materials Science) by Clarivate Analysis and Most Cited Chinese Researchers (in Materials Science) by Elsevier in 2016, 2017 and 2018. His current research focuses on design and synthesis of micro-/nanomaterials for electrochemical energy-related applications including supercapacitors, Li/Na/K-ion batteries, Li-S batteries and energy-storage photocatalysts. He has published about 100 papers in peer-reviewed Journals with a total citation of >7,500 times and an h-index of 46.

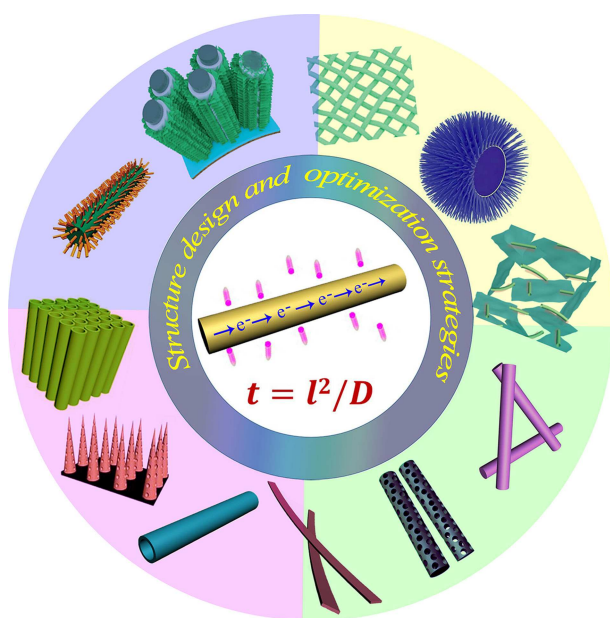
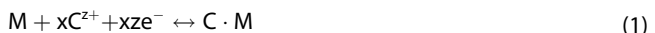


Figure 1. Designed versatile structures and optimization strategies for 1D nanostructured PCMs.

Commonly, the underpotential deposition occurs as the ions deposit on the metal-electrolyte interface at potentials positive to their reversible redox potential,^[4] such as, the H⁺ ions deposit on the Pt and Pd²⁺ on the Au surface.^[41,42] The process is described by the following Equation:^[4]



where *M*, *C*, *x*, and *z* are the noble metal, absorbed atoms, the number of absorbed atoms, the valence of the absorbed atoms, respectively. Other examples, such as Cu or Ag deposited on the Au electrode and Pb on the Ag electrode, are also carried out.^[42] Electrode materials working with the underpotential deposition mechanism is rarely used in the design of super-

capacitors in view of their special emerging background and low SCs.

For typical redox pseudocapacitance, the charges are always stored through electrochemical adsorption of ions on/near the surface of the electrode materials accompanying fast and reversible electron transfer.^[3,4] The reactions can be generally described by the following Equation:^[4]



where C⁺ is the surface-absorbed electrolyte cations (such as, H⁺, Li⁺, K⁺, Na⁺), and *z* is the number of the transferred electrons. Strikingly, RuO₂ and MnO₂ are established as the most two distinct examples for redox pseudocapacitance. Figure 3a shows the schematic cyclic voltammetry (CV) profiles of the MnO₂ electrode in 0.1 M K₂SO₄.^[2] The CV curve shows a rectangular shape, which suggests the successive and highly reversible surface redox reactions taking place in the MnO₂ electrode: MnO₂ + xC⁺ + yH⁺ + (x + y)e⁻ ↔ MnOOC_xH_y.^[2] Similar rectangle-like CV shape is also observed at the case of RuO₂.^[37] Besides, other metal oxides such as TiO₂, Fe₂O₃, as well as CPs have been demonstrated to possess the pseudocapacitive behaviors.^[15,17] Nevertheless, several eminent and/or faint redox peaks lie on CV curves for these electrodes.

By contrast, the intercalation pseudocapacitance is based on the ion insertion/intercalation into the layers and/or channels of electroactive materials without phase transformation.^[4,36] Typically, the process with the Li⁺-insertion/intercalation can be reasonably illustrated as the following Equation:



where MA_y and *x* are the layer-lattice intercalation host material and the number of transferred electrons, respectively. As is well known to all, Nb₂O₅,^[43,44] TiNb₂O₇,^[45] V₂O₅,^[46] MoS₂,^[47] Li₃VO₄,^[48] Li₂TiSiO₅,^[49] and MXenes^[50] are very attractive intercalation PCMs for supercapacitors. Taking the Nb₂O₅ as an example, a pair of reversible redox peaks in CV curves with a scanning rate

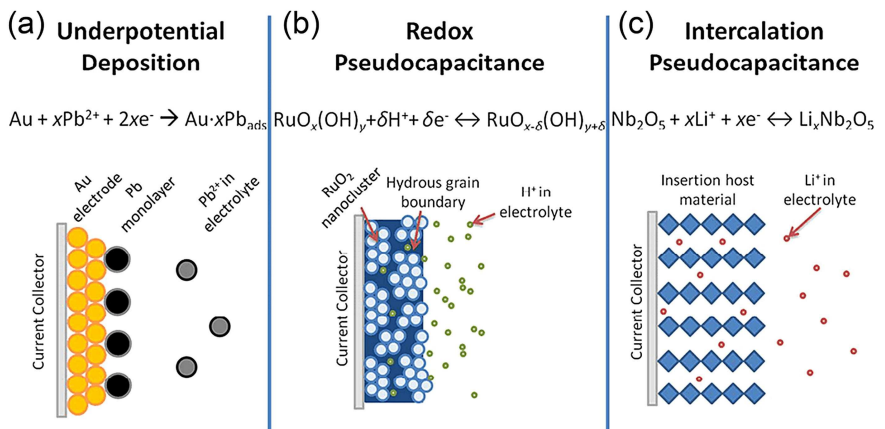


Figure 2. Schematics illustrations for the charge-storage mechanisms for PCMs: a) underpotential deposition, b) redox pseudocapacitance, and c) ion intercalation pseudocapacitance.^[36] Reported with permission from ref 36. Copyright 2014 RSC.

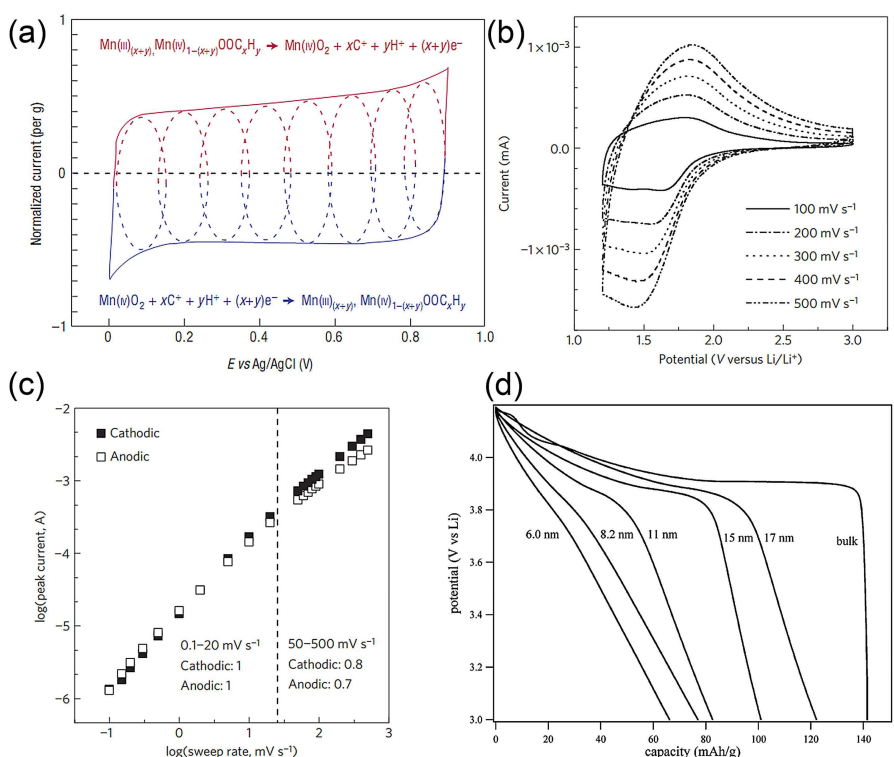


Figure 3. a) Schematic CV profiles of the MnO₂ in 0.1 M K₂SO₄.^[2] Reported with permission from ref 2. Copyright 2008 Nature Publishing Group. Kinetic analysis of the electrochemical behavior of T-Nb₂O₅.^[43] b) CV curves from 100 to 500 mV s⁻¹. c) b-value determination of the anodic and cathodic peak currents shows that this value is approximately 1 up to 50 mV s⁻¹. Reported with permission from ref 43. Copyright 2013 Nature Publishing Group. d) The effect of crystallite size on discharge behaviors of the LiCoO₂.^[53] Reported with permission from ref 53. Copyright 2014 ACS Publication.

from 100 to 500 mV s⁻¹ (Figure 3b) is observed corresponding to the intercalation of Li⁺ ions into the Nb₂O₅: Nb₂O₅ + xLi⁺ + xe⁻ ↔ Li_xNb₂O₅.^[43] Figure 3c depicts the plot of log(*i*) versus log(*v*) from the sweep rates of 0.1 to 500 mV s⁻¹. According to the relationship of voltammetric response (*i*) and sweep rates (*v*):^[44]

$$i = av^b \quad (4)$$

where *a* and *b* are adjustable parameters. The *b*-value determination of the anodic and cathodic peak currents shows that the value is approximately 1.0 up to 50 mV s⁻¹, indicating that the charge storage is typically capacitive for the Nb₂O₅.^[43] As well noted, the *b* value is a decisive factor to differentiate the PCMs and battery-type materials. As for the battery-type process (*b*=0.5), the reactions can occur in the bulk and are limited by solid-state diffusion, while the *b* approaching 1.0 implies the pseudocapacitance-controlled reaction.^[36,38] Thus, as for the materials with partial capacities contributed by pseudocapacitance, the relationship of *i* and *v* can be depicted as follows:^[36]

$$i = k_1 v^{1/2} + k_2 v \quad (5)$$

By calculating the values of *k*₁ and *k*₂, it is highly rational to distinguish the specific contribution proportion of the diffusion and capacitive processes.^[51] Another feature to distinguish the capacitive behavior is that the PCMs show either rectangle-

shape CVs or little difference between the anodic and cathodic peaks in the CVs, while the battery-type materials visually present distinct peaks in CVs and typical platforms in the charge-discharge profiles.^[51,52]

In general, those PCMs with typical capacitive characteristics are considered as the intrinsic nature, and explored extensively in a wide range of morphologies and particle sizes. By contrast, some metal oxides, which display battery-like behaviors in the bulk state but deliver capacitive features through nanostructuring, are established as the extrinsic PCMs.^[36] For instance, Honma et al. investigated the nanosize effect on the Li-ion intercalation properties of the LiCoO₂ electrode.^[53] As shown in Figure 3d, the bulk LiCoO₂ exhibits a typical plateau at ~3.9 V during the Li⁺ insertion. With the crystallite size decreasing from 17 to 6 nm, the capacitive properties became more and more dominant. The transformation to capacitive behaviors can be ascribed to the nanosized effect, which improves the surface Li-ion storage of the nano-LiCoO₂. With nanostructuring, the materials are endowed with the increasing surface area and shortened diffusion/transport distance, and the enhanced rate capabilities are obtained accordingly.^[36,53] Therefore, the pseudocapacitance can be realized when an electrode is engineered down to nano-size dimensions, where substantial Li ion storage sites on/near the surface will be achieved for the case. Besides the battery-type LiCoO₂, other battery materials, such as nickel and cobalt hydroxides, also exhibit favorable rate performance and good cycling stability in nanosized structures, which provide abun-

dant active sites and shorter ions diffusion distance.^[54] As a result, these Ni/Co-based compounds can be utilized to couple with capacitive materials (such as activated carbons) to fabricate high-specific-energy-density hybrid supercapacitors.

Up till now, the in-depth understanding of the charge storage mechanisms of PCMs has been an everlasting topic in supercapacitors, especially the use of advanced *in/ex-situ* spectroscopic techniques for newly electroactive materials and the influence of the nanostructures on the capacitive performance including the SCs, cycling performance, and so on. Yuan et al. reported the electrooxidation-generated new phases of CoOOH/NiOOH that contribute to the exceptional pseudocapacitance observed after CV cycles from conductive NiCoSe₂ hollow sub-microspheres through post analysis (XRD, XPS, TEM) of the cycled electrode.^[15] Furthermore, the cycled NiCoSe₂ electrode still maintains its hollow feature, which accounts for its desirable cycling stability. In addition to the electrochemically induced phase transformation mechanism, the morphology and microstructure change (such as, aggregation, structural collapse, and so on), the interfacial reactions of electrodes during the charge storage process further greatly influence their cycling performance.^[54] These results will offer profound understanding of the pseudocapacitive process. Furthermore, Liu and co-workers reported the phase evolution of $\alpha\text{-Mn}_{0.98}\text{O}_2$ using *ex-situ* and in operando Raman spectroscopy, which indicates that the $\alpha\text{-Mn}_{0.98}\text{O}_2$ can be converted to MnO₂ and Mn₃O₄, and both the phases render the energy storage process through the reversible phase transform, which involves the hydrated cations Na⁺, protons H⁺ and Mn²⁺ intercalation/de-intercalation in the charge-discharge process.^[55] In addition, the systematic in operando Raman spectroscopic study of thin-film NiO₂H_x reveals that the breaking/formation of O–H bond plays a major role in charge storage while the insertion/extraction of cations provides much less contribution.^[56] The investigation in the correlation between structural changes and electrochemical properties will help to probe new insights into the fundamental charge storage mechanism of the PCMs.^[54] Overall, appropriate evaluation of the electroactive materials and their charge storage mechanisms will facilitate the huge progress in this burgeoning field of electrochemical energy storage.

Physicochemical Properties and Merits of 1D Nanostructured Materials for Supercapacitors

Recently, 1D nanostructured materials have received increasing interests because of their distinctive virtues and wide range of potential applications.^[19] Normally, 1D nanostructured materials have a high aspect ratio (length/diameter), large specific surface area (SSA) and quantum confinement effect, together with unique electrical, optical, photovoltaic and mechanical properties, making them appropriate for various applications of biosensors, solar cells, photodetectors, field emissions, and energy conversion and storage.^[32,34] For electrochemical energy storage applications, especially supercapacitors, 1D nano-

architectures themselves are endowed appealingly with several advantages as follows:

- 1) It can shorten the electronic pathways, facilitating electrical transport in the axial direction compared with their bulk counterparts.^[57,58]
- 2) In 1D nanostructured electrodes, the ion diffusion length is shortened, which will benefit for the rate capability, according to the relationship of the characteristic time (*t*) for ions diffuse through the electrode with the diffusion length (*l*) and diffusion coefficient (*D*): $t \approx l^2/D$.^[31,59]
- 3) 1D nanostructures possess large electroactive SSA increasing the electrode/electrolyte contacting sur-/interfaces, which further enhances electrode kinetics with ultrafast charge-discharge capability.^[60,61]
- 4) 1D nanostructures can *in-situ* grow on the conductive substrates, and further form uniform nanoarrays, which realizes binder-free electrode and prevents the nanostructures from conglomerating.^[62]
- 5) 1D nano-architectures can easily form several higher level multi-dimensional structures with improved SSA and good mechanical stabilities for enhanced SCs and cycling performance.^[63,64]

Preparation and Formation Mechanism of 1D Nanostructured PCMs

As we all know, the morphologies, dimensions, compositions, and atomic structures are strongly associated to their electrochemical performance of electrode materials. Numerous contributions over the past years have been devoted to investigating the growth mechanisms and controlling specific parameters of 1D nanostructured materials.^[34,65] A variety of physical and chemical methods have been explored including hydrothermal/solvothermal strategy, electrochemical deposition, electrospinning methods, vapor deposition, sol-gel route, template-assisted method, and so on. All the approaches to 1D nanostructured materials can be mainly categorized into two major strategies: bottom-up and top-down.^[34,66,67] The former is usually considered as the low-cost and effective approach for 1D materials,^[34,66] in which electroactive materials arise from the individual atoms/molecules, and further assemble into the desired structures and morphologies. And the latter is that the entire part is fully changed into small segments by different methods such as lithography, ball milling, etching, and so on.^[34,67] One should note that the combination strategies are often adopted in many instances, that is, a “bottom-up” approach to fabricate the 1D backbone and then a “top-down” avenue to create some unique nanostructures on it, such as pore or hollow regions in/on it.^[18] Based on the synthetic methodologies, various 1D nanostructured materials with versatile structures and morphologies can be designed and synthesized, such as NWs, NTs, NRs, NBs and NFs.^[18,34] And herein, we mainly focus on the methods which can be utilized to build 1D nanostructured materials of pseudocapacitive properties.

Hydrothermal/Solvothermal Methods

Hydrothermal/solvothermal method is most widely applied for the fine fabrication of 1D nanostructured PCMs in term of its highly dispersible, size-controllable, effective, and high-yield properties.^[34] Hydrothermal/solvothermal strategies can create unstable crystalline phase at the melting point. The formation of crystal always undergoes three stages including the formation of the supersaturated solution, nucleation, and crystal growth.^[65,66] Or said slightly differently, the precursors and possibly the reagents capable of regulating and/or templating the crystal growth with an appropriate ratio are added into the water or organic solvents including the alcohol, ethylene glycol (EG), N, N-dimethylformamide (DMF), diethylamine (DEA), oleylamine or even water/organic mixtures.^[66,67] Then, the mixture is transferred into an autoclave with the elevated temperatures and pressures. During the hydrothermal/solvothermal process, the reaction is accelerated, and small clusters are formed via fast and homogenously nucleated process as the monomers such as atoms, ions or molecules appear even higher than their saturation.^[34] Then, the formed clusters function as crystalline seeds for further growth to form large nanostructures. Finally, the target 1D nanostructured PCMs are formed via Ostwald ripening as the main process after the nucleation and growth.^[68–70]

The crystalline structures and morphologies of 1D nanostructured PCMs can be easily controlled by altering the hydrothermal/solvothermal parameters, such as pressures, temperatures, and adjusting the precursors' ratios and additive amount. In some cases, the capping molecules or surfactants are added to change the free energies of crystallographic surfaces and orient along with defined crystal planes to form the 1D structures with good crystallinities, homogenous composition, or even some porous or hollow structures.^[18] Benefiting from the synthetic advantages mentioned above,

lots of 1D PCMs have been successfully synthesized through the hydrothermal/solvothermal methods, such as MnO_2 ,^[71] V_2O_5 ,^[72] WO_3 ,^[73] RuO_2 ,^[74] MoO_3 ,^[75] Nb_2O_5 ,^[76] Fe_2O_3 ,^[77] Co_3O_4 ,^[78] TiO_2 ,^[79] SnO_2 ^[80] and so on. Figure 4a, b show the as-obtained TiN NW arrays on carbon fabric substrate, which are fabricated through hydrothermal treatment by Li and co-workers.^[81] Additionally, porous CoO NWs on Ti substrate (Figure 4c)^[82] are prepared by Jiang et al. and single-phase $\alpha\text{-MnO}_2$ NWs (Figure 4d) by Mahanty et al.^[83] Overall, the hydrothermal/solvothermal methods for 1D nanostructured PCMs have been well-established protocols with the appealing merits including simplicity, controllability, low cost and environmentally friendly characterizations. Notably, 1D nanostructured materials achieved by hydrothermal/solvothermal method sometimes possess low conductivity and poor pseudocapacitive performance, which probably results from their poor purity and low crystallinity. So further treatments, such as surface modifications, annealing, coating, and even doping, are usually needed.

Electrochemical Deposition

Electrodeposition methods have been employed intensively to synthesize pseudocapacitive nanostructured materials including metal oxides and CPs. Electrochemical deposition is a oxidation or reduction process to accumulate desired coating of a metal, oxide or salt onto the surface of a conductive substrate.^[84] Thus, the electrodeposition is usually considered as a simple, mass-productive, controllable, economic and environmentally friendly method. By altering the electrodeposition parameters (current, potential, pulse modes, electrolyte composition, etc.), 1D nanostructured PCMs with various morphologies including NRs,^[84] NTs,^[85] nanoneedles,^[86] and NWs^[87] have been fabricated. For instance, Mai et al. electro-deposited the worm-like MnO_2 NWs onto carbon fabric by an

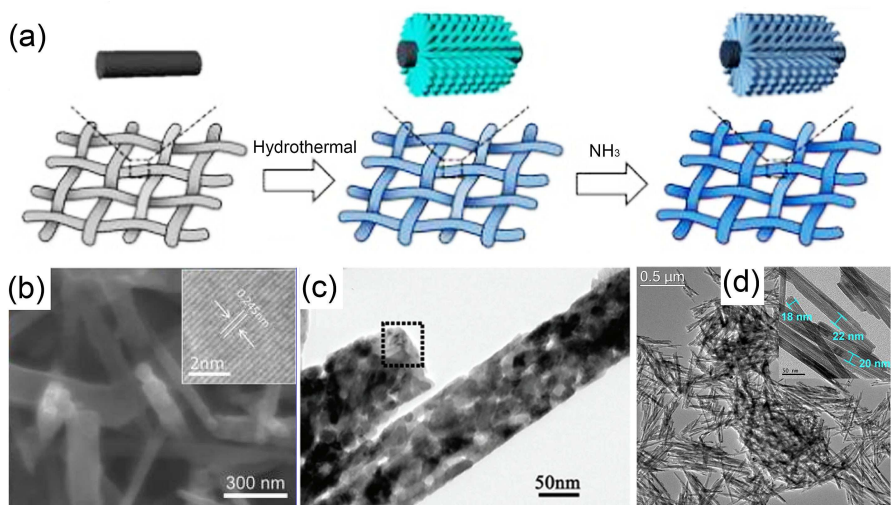


Figure 4. a) Schematic illustrations for the preparation of TiN NWs on carbon cloth substrate. b) FESEM image of TiN on a single carbon fiber (the inset for the lattice-resolved TEM image).^[81] Reported with permission from ref 81. Copyright 2012 ACS Publication. c) TEM image of CoO NWs on Ti substrate.^[82] Reported with permission from ref 82. Copyright 2010 ACS Publication. d) TEM image of hydrothermal synthesized $\alpha\text{-MnO}_2$ NWs.^[83] Reported with permission from ref 83. Copyright 2014 ACS Publication.

anodic electrodeposition process. When utilized as a flexible electrode, the resultant MnO₂ NWs demonstrate attractive electrochemical capacitances towards supercapacitors.^[87]

As well retrieved, several CPs (PANI,^[88] PPy,^[89] and PEDOT^[90]) with 1D nanostructures have been template-free electrodeposited on various conductive substrates including carbon fibers, conductive carbon paper, or metal plate. Additionally, the well-defined 1D PCMs also can be achieved by the templates, such as the anodic aluminum oxide (AAO), ZnO NWs, or other metal NWs.^[62] Furthermore, 1D nanostructured metal oxide heterojunctions or metal oxide/polymer coaxial NWs can be purposefully fabricated by multi-step electrodeposition or electrochemical co-deposition,^[91] highlighting the enormous capabilities of electrodeposition methods to design more complicated and/or even hybrid 1D PCMs for supercapacitors.

Electrospinning

Electrospinning is extensively conducted to electrostatically and continuously generate fine fibers with diameters from nanometer to micrometer, starting from the liquid precursors.^[92] Electrospinning always shows the unique and flexible capabilities for the continuous production of NFs with controllable compositions, colorful structures, and specific textures.^[34,62] Various materials including polymers, composites, semiconductors and ceramics can be transformed into fibrous nanostructures by the electrospinning technique. As noted, the conventional electrospinning set-up in lab is a low-cost and effective equipment, which is commonly made from three major components: a high voltage (kV) power supply, a spinneret (a syringe or pipette tip) and a grounded collector (typically a metal plate or a rotating mandrel). Typically, as a high voltage (5–30 kV) is applied to the solution, a jet erupts from the tip of the spinneret producing a repulsive force (larger than its surface tension) within the charged solution, and then the electrified jet undergoes a stretching and whipping process, dries in flight, and eventually the as-formed fibers are deposited on the grounded collector.^[92,93] By regulating the parameters such as the applied voltage, environmental humidity/temperature, solution viscosity/component, and the distance between the spinneret tip and collector, the specific diameters, lengths and structures of the as-resulted fibers can be easily controlled.^[92] 1D NFs and their-constructed two-dimensional (2D) membranes/three-dimensional (3D) fabrics can be achieved easily by virtue of the tremendous varieties of the electrospinning in materials, structures, architectures and functionalities.^[92,93]

In most cases, the precursors are usually added into the solvent (such as water, alcohol, DMF) to form a homogeneous and viscous mixture, then continuous spun fibers are produced and collected with electrospinning.^[92,94] The electrospun fibers are composed with polymers, such as polyvinyl pyrrolidone, polyacrylonitrile, polyvinylidene fluoride, and precursors, and they are not used directly as the electrode materials. Electrospinning is only a key process for fabricating 1D nanostructured PCMs, and the subsequent annealing process is always

necessary. Under the inert atmospheres, the precursors can be converted into the pseudocapacitive nanostructured materials embedded into and/or on the surfaces of conductive carbon matrixes derived from the polymer precursors. Otherwise, under the oxygen atmosphere, the polymers are whole burn out, and pure PCMs with meso-/microporous structures are provided accordingly. Through optimize the annealing parameters including heating rate, atmosphere and preheating, the fibrous structures can be obtained. Recently, Wang et al. explored the electrospinning method to prepare the Li₂TiSiO₅/carbon (LTSO/C) fibrous electrode with the unique 3D interconnected nanoarchitecture consisting of aggregation-free LTSO nanoparticles (Figure 5).^[49] Electrochemical test further confirms that as-synthesized LTSO/C electrode shows the high-rate pseudocapacitive Li⁺-storage properties, as expected. Zhu et al. designed an advanced architecture of TiO₂@CNT@C NRs by the electrospinning method. The TiO₂@CNT@C electrode shows excellent cyclic stability and outstanding rate capability in half cells.^[95] Corresponding kinetic analysis demonstrates that the contribution from the extrinsic pseudocapacitance of the TiO₂@CNT@C NRs affects their rate capabilities to a large extent. Overall, the electrospinning is a highly efficient avenue to obtain 1D PCMs with fibrous structures, benefiting for rapid charge transfer and reduced ion diffusion/transport path in electrochemical processes.

Vapor-Based Methods

Vapor deposition is another common way to synthesize high-quality 1D nanostructured PCMs. Vapor deposition usually operates in vacuum and under high temperatures. Several vapor deposition techniques including the chemical/physical vapor deposition, atomic layer deposition (ALD) and pulsed laser deposition have been intensively explored.^[96,97] Vapor deposition provides distinct advantages in fabricating 1D PCMs compared to wet chemistry methods. For example, the working conditions, such as high-temperature and high-vacuum deposition, guarantee the 1D nano-dimensional PCMs with high-quality crystallinity.^[66] In addition, by adjusting the technique parameters including precursors, catalysts, growth sites, temperatures, or pressures, 1D nano PCMs with distinct structures, dimensions, locations, compositions, and organizations can be well controlled.^[65,96] Moreover, the controllable growth theories of semiconductor NWs/films can be adopted for the in-depth understanding of the growth behaviors of 1D PCMs over the vapor deposition. Zhang et al. fabricated a core-shell structure of ZnO/Ni NW arrays via ALD synthesis of Ni layer coating on ZnO NWs, which delivered superior capacitive properties including high SCs, good rate performance and long cycling stability.^[98] However, vapor deposition is generally labeled with high-cost, time-consuming, complex-process and small-scale production.

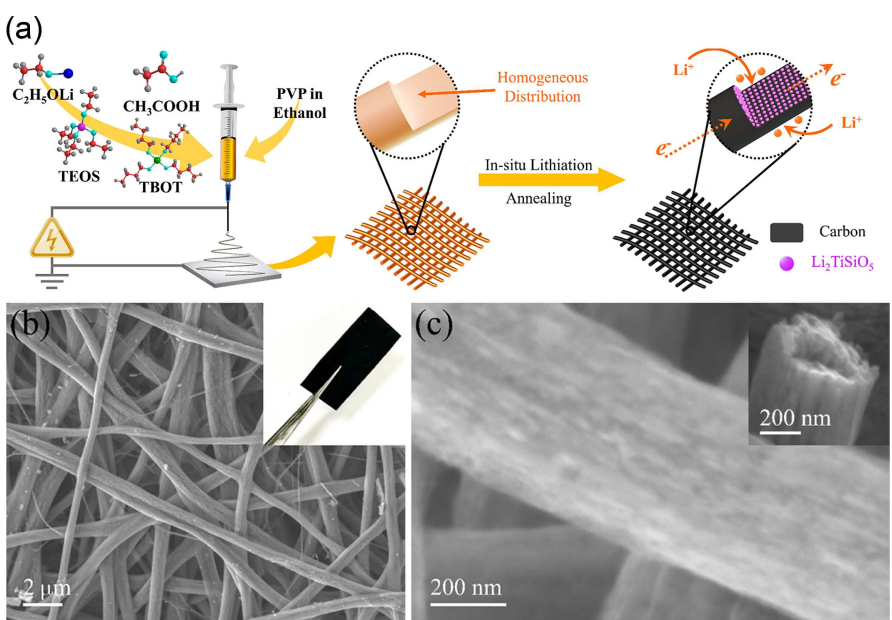


Figure 5. a) Schematic of the synthetic process of LTSO/C NFs. b), c) SEM images of the LTSO/C NFs (inset in b is the optical photograph of the LTSO/C film).^[49] Reported with permission from ref 49. Copyright 2019 Elsevier.

Other Methods

Besides the mostly used synthetic methodologies mentioned above, other strategies including sol-gel method, chemical etching, microwave assisted method, lithographically patterned method, and so on, have been reported for designing 1D nanoscaled PCMs.^[18,99,100] In particularly, Yuan et al. reported the electrochemically induced formation of *bi*-component electroactive NiOOH/CoOOH nanowiskers (2 nm in diameter) over CV cycling for asymmetric supercapacitors as a positive pseudocapacitive electrode.^[100] Practically, it is quite common for two or even multiple methods of use to be applied for synthesizing certain nanostructures, rather than any single one.

The Applications of 1D Nanostructured PCMs in Supercapacitors

As aforementioned, 1D nanostructured materials with attractive advantages can be smartly fabricated via lots of synthetic strategies for supercapacitors. In this section, several examples will be presented in detail to understand the fabrication and applications of 1D nanostructured PCMs in advanced supercapacitors.

Conventional 1D Nanostructures for Supercapacitors

The conventional 1D nanostructured materials with distinct morphologies like NWs, NRs, NFs, NBs, nanoribbons, nanobristles, and so on, have been attracted great interests thanks to their unique merits, as discussed above.^[23,101–106] Various

PCMs (MnO₂, V₂O₅, Co₃O₄, MoO₃, PANI, etc.) with 1D nanoarchitectures have been widely investigated.^[25,102,107–109] Mesoporous MnO₂ NWs were synthesized by the lithographically patterned NW electrodeposition method (Figure 6a).^[110] The height and width of the MnO₂ NWs are well controlled in the range of 21–63 nm (height) and 200–600 nm (width). The largest SC measured by the CVs of the MnO₂ NWs is 923 Fg⁻¹ at a scanning rate of 5 mV s⁻¹. Binary metal oxides, usually possess much better electronic conductivity than that of any single component, and higher electrochemical activity, are of huge potential for pseudocapacitors. Yuan et al. proposed the hydrothermal fabrication of 1D ultralayered mesoporous NiCo₂O₄ NWs,^[111] which are constructed from quasi-single-crystalline nanosheet building blocks. Benefiting from the unique ultralayered mesoporous architecture and binary Co/Ni electroactive sites, the as-obtained NiCo₂O₄ NWs exhibits high SCs, good rate capability, and long cycling life. Yu and co-workers reported a molten-salt method to prepare ultralong MnO₂ NWs.^[112] After doping with different transition metal ions, the FeMnO, CoMnO, NiMnO, and CuMnO NWs are obtained with a diameter of approximately 40 nm and an average length of 10 μm, as well as uniform single crystal structure (Figure 6b–e). Benefiting from novel single-crystal nanostructure and hetero-ions doping induced enhanced electronic conductivity, the MnO₂-based NWs display greatly improved SCs and excellent cycling performance. Porous VN NWs were prepared by a simple hydrothermal method, followed by an annealing process at 600 °C for 1 h in ammonia atmosphere.^[113] As shown in Figure 7a, b, the obtained VO_x precursor with smooth surface shows a diameter in the range of 300–800 nm and length up to tens of micrometers. After high-temperature nitridation, VN NWs are obtained with a single crystalline porous structure (Figure 7c). When utilized as negative material in an asymmetric

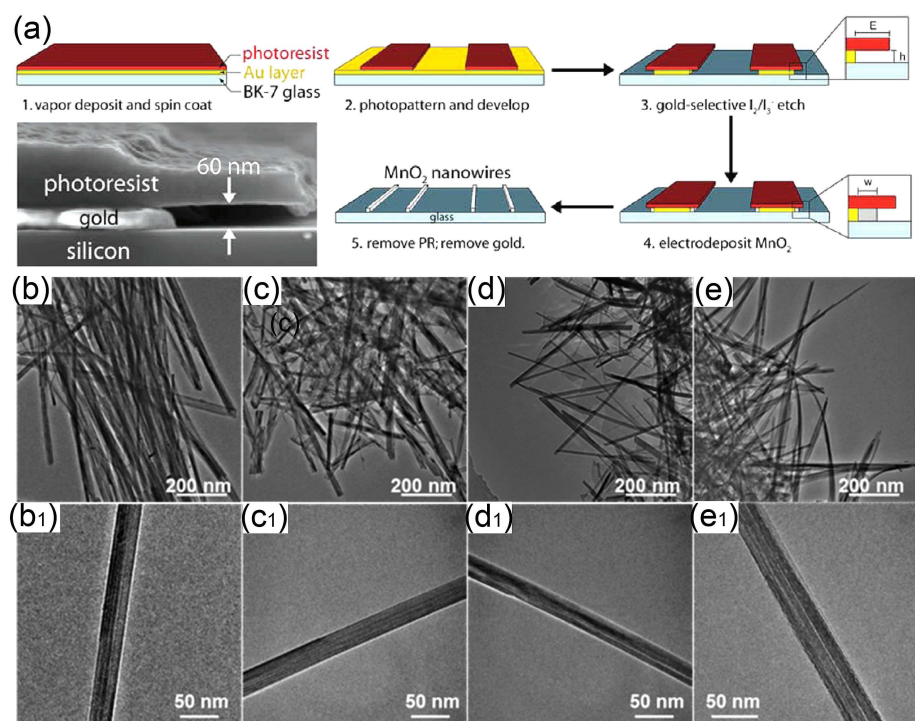


Figure 6. a) Schematic diagram for the electrodeposition of MnO_2 NWs using the lithographically patterned NW electrodeposition method (the lower left inset for the SEM image of a gold electrode and produced trench structure).^[110] Reported with permission from ref 110. Copyright 2011 ACS Publication. TEM and HRTEM images of b), b1) FeMnO, c), c1) CoMnO, d), d1) NiMnO, and e), e1) CuMnO.^[112] Reported with permission from ref 112. Copyright 2016 ACS Publication.

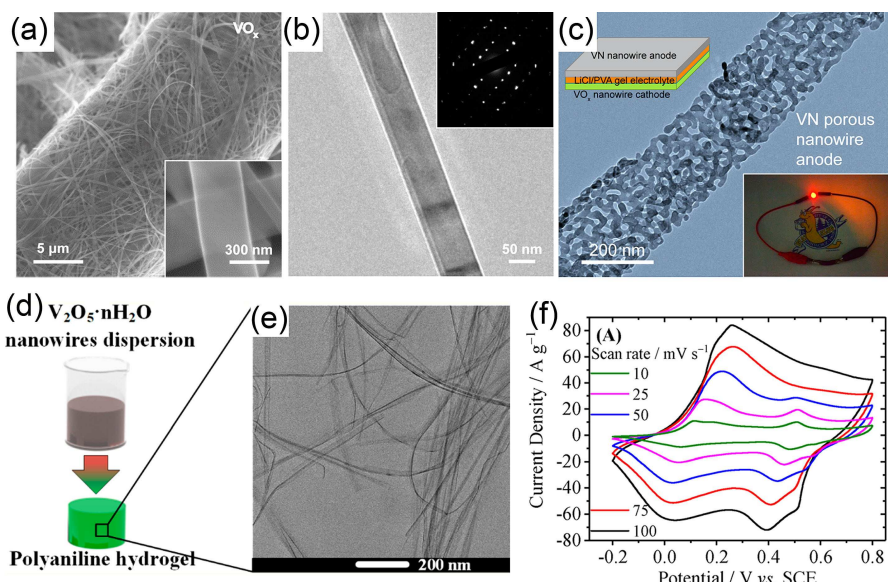


Figure 7. a) SEM image of VO_x NWs (the inset for the magnified SEM image of the NWs). b) TEM image of a VO_x single NW (the inset for the SAED pattern). c) TEM image of the porous VN NW (the inset for the fabrication schematic of the asymmetric supercapacitor and optical photograph of a LED powered by the fabricated device).^[113] Reported with permission from ref 113. Copyright 2013 ACS Publication. d) Schematic illustration of the fabrication route of pure PANI hydrogel. e) TEM image of the PANI NFs. f) CV curves of PANI electrode in 1 M H_2SO_4 .^[101] Reported with permission from ref 101. Copyright 2018 ACS Publication.

cell, the VO_x/VN device exhibits a stable potential window of up to 1.8 V and excellent cycling performance with only 12.5% of SC degradation after 10000 cycles.

Apart from the transition metal compounds, 1D nanostructured CPs also have drawn considerable attentions due to their high electronic conductivity and electrochemical performance.^[101] Typically, the PANI NFs are fabricated through

an *in-situ* polymerization process using the $\text{V}_2\text{O}_5\text{-nH}_2\text{O}$ NWs as both the sacrifice template and oxidant, and render an extreme aspect ratios with an average diameter of only 3.4 ± 0.8 nm.^[10] The ultrathin feature of the NFs allows the formation of hydrogels during the *in-situ* polymerization process. Schematic illustration for the fabrication of the PANI hydrogel, and corresponding scanning electron microscopy (SEM) image of the PANI NFs are shown in Figure 7d–e. The ultrathin nature of NFs and large porosity of the PANI hydrogel stimulate fast diffusion of electrolytes both between and inside the NFs, thus favoring for the remarkable supercapacitive properties. According to the electrochemical tests (Figure 7f), The PANI hydrogel achieves large SCs of 636 F g^{-1} at 2.0 A g^{-1} , and 626 F g^{-1} at 25.0 A g^{-1} , as well as good cycling performance with 83.3% of SC retention after 10000 cycles.

Other 1D nanostructures, such as NRs, NTs, and NBs, have been extensively studied for their applications in supercapacitors.^[114–117] The CoP NRs (Figure 8a) are prepared by simply thermal decomposition of the cobalt acetylacetone in oleylamine system with triphenylphosphine as phosphorus source, and display a SC of 284 F g^{-1} (198.8 C g^{-1}) along with good rate capability.^[114] Hou et al. have developed an efficient template-free strategy for synthesizing monoclinic $\text{Co}_2\text{P}_2\text{O}_7$ NRs towards high-performance supercapacitors, and propose the possible charge storage mechanisms of the $\text{Co}_2\text{P}_2\text{O}_7$ NRs in KOH electrolyte.^[115] Yan and co-workers reported the oxidation-etching preparation of MnO_2 NTs (Figure 8b).^[116] The optimized nanotubular structure delivers high SCs of 461 F g^{-1} at 5 mV s^{-1} and 248 F g^{-1} at 100 mV s^{-1} , and excellent cyclability with no obvious SC decay during 3000 charge-discharge cycles. Tong et al. carried out a facile electrodeposition process to synthesize Bi_2O_3 NBs (Figure 8c), and systematically investigated their capacitance properties.^[117]

Although 1D nano electrodes have some unique merits for electrochemical energy storage, they are still faced with several non-ignorable challenges, which significantly affect the ultimate performances of electrochemical devices. For instance, nano-materials intrinsically have strong self-aggregation tendency, resulting from their large surface energy, which potentially impedes the electrolyte diffusion into the electrode. Besides, the nanoscaled electrodes often suffer from the structure degradation during the charge-discharge processes, leading to the poor cycling performance of the full cells to

some extent. Thus, to meet the rigid demands of large SCs, good rate capability, and excellent cycling performance for the PCMs, further optimized strategies of the traditional 1D nanostructured PCMs still should be contrapuntally exploited.

1D Nano-Arrays for Supercapacitors

To improve electrochemical properties of 1D PCMs, enormous efforts have been devoted to innovative nanostructure design. Remarkably, the nano-arrays, which are constructed by 1D nano-blocks grown vertically on the substrates (i.e., carbon fabrics, nickel foams, Ti plate, indium tin oxide /fluorine-doped tin oxide glasses, CNTs/graphene papers, and so on), have attracted great attentions for elegantly designing high-performance PCMs towards advanced supercapacitors.^[118–120] The nano-arrays often render an open yet ordered space for rapid diffusion of electrolytes into the inner electrode. Moreover, the nano-arrays directly grown on the substrates with robust adhesion avoid the use of insulating binder and guarantee the expressway for electron transport.^[25]

Vertically aligned CPs nano-arrays are known as an appealing electrode for supercapacitors. Wei et al. fabricated uniform PANI NW nano-arrays through a one-step template-free galvanostatic current method,^[121] as shown in Figure 9a. Since the vertically aligned nanostructure favors for the ion diffusion into the inner electrode, as schematically depicted in Figure 9b, the PANI NW arrays illustrate a large SC of 950 F g^{-1} at 1 A g^{-1} , and keep it as high as 780 F g^{-1} even at super high rate of 40 A g^{-1} . Besides this, the oriented PPy NW arrays with a diameter of $80\text{--}100 \text{ nm}$ and a length of $1\text{--}4 \mu\text{m}$ are also developed for their application in supercapacitors.^[122] The PPy nano-arrays obtains a SC of 566 F g^{-1} , much better than the previous reported disordered PPy NWs and bulk electrodes. Furthermore, the PEDOT NT arrays were electrochemically synthesized using an alumina template membrane.^[90] Figure 9c shows the transmission electron microscopy (TEM) image of a single PEDOT tube. The tubular architecture with open space and thin walls (Figure 9d) allows the counter ions readily to penetrate into the internal electrode, and shortens the diffusion distance in the electrode. Accordingly, the PEDOT NT arrays based symmetric supercapacitor demonstrates a high power density of 25 kW kg^{-1} .

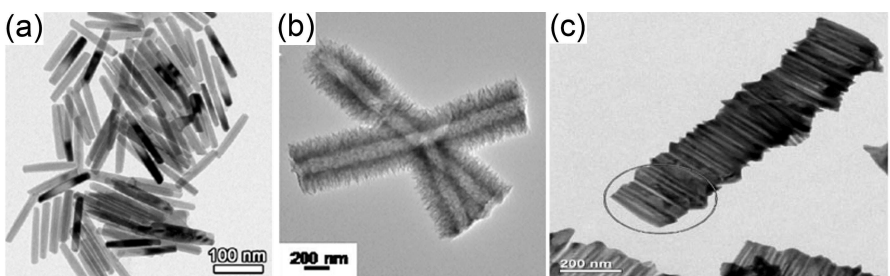


Figure 8. a) TEM image of CoP NRs.^[114] Reported with permission from ref 114. Copyright 2016 ACS Publication. b) TEM image of MnO_2 NTs.^[116] Reported with permission from ref 116. Copyright 2018 ACS Publication. c) TEM image of Bi_2O_3 NBs.^[117] Reported with permission from ref 117. Copyright 2010 RSC Publication.

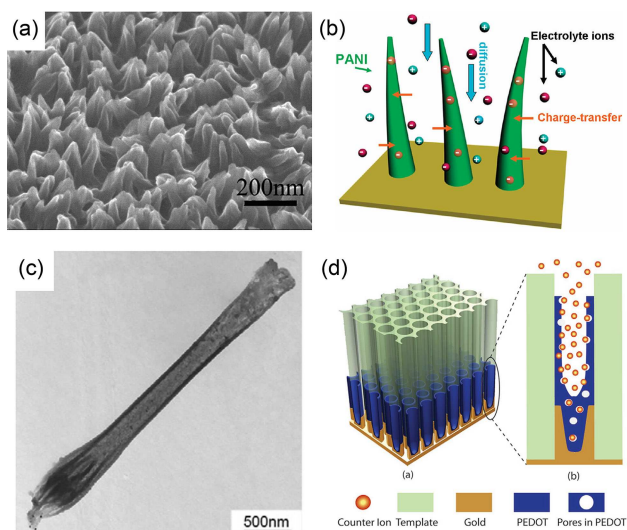


Figure 9. a) SEM image of the PANI NW arrays. b) Schematic illustration for the ions diffusion path in NW arrays.^[121] Reported with permission from ref 121. Copyright 2014 ACS Publication. Electrode made of PEDOT NTs in a porous alumina template: c) TEM image of PEDOT NTs synthesized in 20 mM EDOT at 1.6 V with a charge density of 200 mC cm⁻². d) Schematic of ion transport (doping or charging) in a single NT.^[80] Reported with permission from ref 80. Copyright 2008 IOP Publishing.

Transition metal oxides, sulfides, nitrides, and other related compounds have also been fabricated to 1D nano-array structures for supercapacitors, such as TiO₂ NTs,^[102] MnO₂ NWs grown on carbon fabrics,^[71] MoO_x NR arrays,^[123] Fe₂O₃ NR arrays,^[124] Co₃O₄ NW arrays^[125] and so on. Efforts on 1D nano-array structures have provided meaningful guidance and new thoughts for fine design and controllable fabrication of the high-performance PCMs. Li et al. reported the anodized fabrication of vertically oriented hydrogenated TiO₂ NTs with striking capacitive behaviors.^[126] Zhang and co-workers devised the fabrication of self-doped TiO₂ NT arrays through the cathodic polarization process on pristine TiO₂ nano-arrays,^[103] as shown in Figure 10a. Electrochemical results indicate that the self-doped TiO₂ NT arrays achieve an enhanced areal SC of 1.84 mF cm⁻², coupled with excellent cycling behaviors.

Wang reported the fabrication of a solid-state asymmetric supercapacitor by using the MnO₂ NW and Fe₂O₃ NT arrays as positive and negative electrode, respectively.^[71] The growth process of nano-arrays and device fabrication are illustrated in Figure 10b. Given the high interfacial area and short ion diffusion path of the nano-array architectures, both the electrodes exert promising energy storage properties. Encouragingly, the as-fabricated asymmetric device manifests a high volumetric energy density of 0.55 mWh cm⁻³ and a long-term stability with 84% of capacitance retention after 5000 continuous cycles. Owing to the congenital advantages, i.e., high theoretical SC (3625 F g⁻¹), low cost, and easy synthesis, Fe₂O₃ holds the great potential as a negative electrode for hybrid supercapacitors. Many researches have been conducted to develop nanostructured Fe₂O₃ materials towards supercapacitors. For example, Tong and co-workers synthesized oxygen-deficient Fe₂O₃ NR arrays distributed uniformly on the carbon fabric

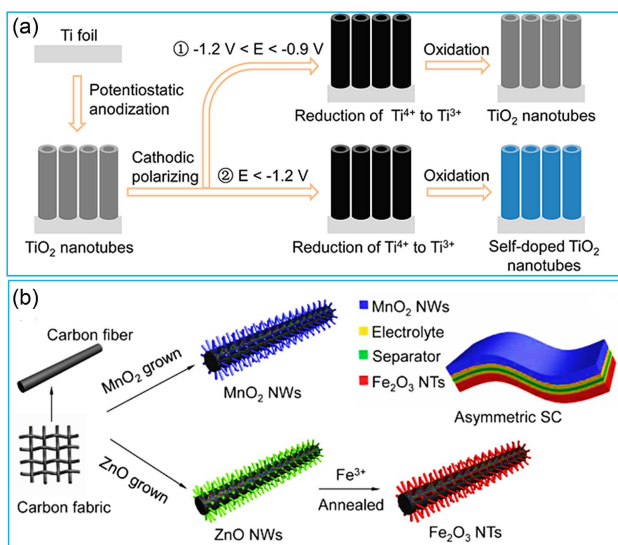


Figure 10. a) Schematic illustration for the fabrication process of the self-doped TiO₂ NT arrays.^[103] Reported with permission from ref 103. Copyright 2014 ACS Publication. b) Schematic diagram illustrating the synthesis procedure of MnO₂ NWs and Fe₂O₃ NTs on carbon cloth.^[71] Reported with permission from ref 71. Copyright 2014 ACS Publication.

(Figure 11a), and the resultant Fe₂O₃ NRs possess a porous and polycrystalline structure (Figure 11b).^[124] Thanks to the synergistic contributions from the fast charge transport and small contact resistance of nano-arrays and favorable oxygen vacancies in the Fe₂O₃ NWs, the oxygen-deficient Fe₂O₃ arrays display a high areal SC of 382.7 mF cm⁻² at 0.5 mA cm⁻² and good cycling stability (Figure 11c).

Other 1D nano-array PCMs such as WON NWs,^[127] Nb NWs,^[27] CoSe NWs,^[128] bimetallic compounds (ZnCo₂O₄, Co-MoO₄, MnCo₂S₄),^[129–131] and so on, have been investigated for their promising applications in supercapacitors. All of these works demonstrate that 1D nano-array PCMs effectively improve the ion diffusion and charge transfer of the electrode itself, thus resulting in high-rate capabilities. Obviously, although some challenges (e.g., enough mass loading are needed to obtain high volumetric energy density while keeping sufficient space for the transportation of electrolyte) are required to be well resolved, the novel array design offers a very promising strategy for next-generation supercapacitors.

1D Core-Shell Nano-Architectures for Supercapacitors

Compared to the single phase PCMs, the binary and/or multiple composites constructed 1D core-shell nano-architectures often benefit from the synergistic effect between the different components to fulfill their application in supercapacitors. As well known, 1D carbon nanotubes (CNTs) hold excellent conductivity, good mechanical properties and high SSA.^[132] Various researches have been reported by employing the CNTs as a backbone to interact with other PCMs for constructing the core-shell nano-architectures.^[132–134] On one hand, CNTs provide good electronic conductivity and enhance the mechanical

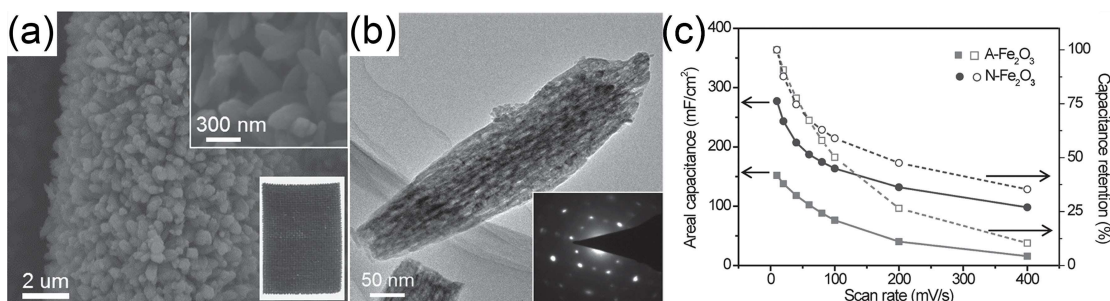


Figure 11. a) SEM image of the oxygen-deficient Fe_2O_3 NR arrays (The insets for the magnified SEM image and digital graph of the Fe_2O_3 electrode). b) TEM image of the oxygen-deficient Fe_2O_3 NRs (the inset for the corresponding SAED pattern). c) Areal capacitances and capacitance retention of the Fe_2O_3 NR arrays calculated from the CV curves.^[124] Reported with permission from ref 124. Copyright 2014 Wiley.

stability of the composites. On the other hand, the 1D nanostructured CNTs can serve as the scaffold for coating of active materials, offering controllable morphology and size of the composites. Typically, the MnO_2 nanoflakes are coated on the CNTs to build a core-shell $\text{MnO}_2@\text{CNTs}$ structure (Fig-

ure 12a–c).^[135] The positive synergistic effect, i.e., the intimate contact between conductive CNTs and pseudocapacitive MnO_2 , minimizes the contact resistance, making the Faradaic process become much easier. As a result, the obtained core-shell $\text{MnO}_2@\text{CNTs}$ electrode delivers a SC of 201 F g^{-1} , as well as

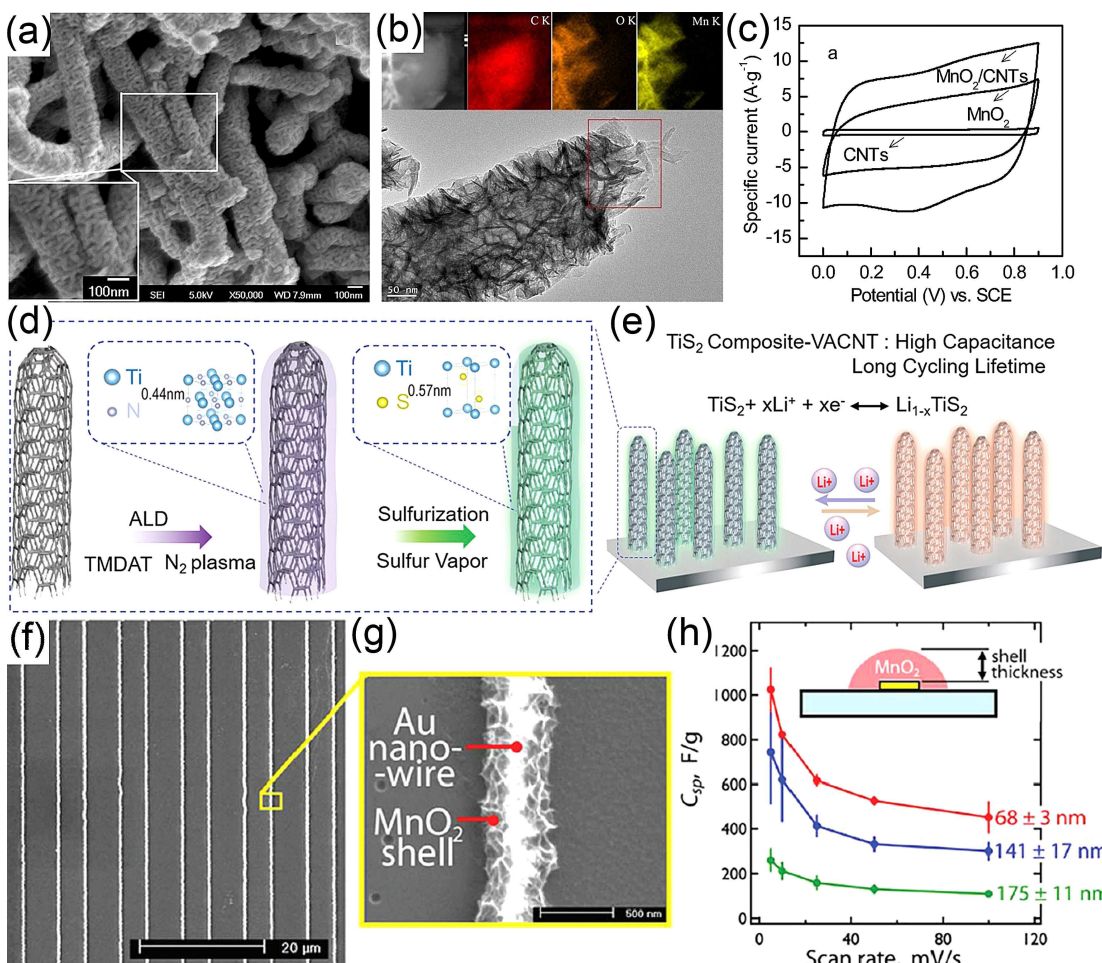


Figure 12. a) FESEM, b) TEM and corresponding elemental mapping images, and c) cyclic voltammetry of the $\text{MnO}_2@\text{CNTs}$ composite.^[135] Reported with permission from ref 135. Copyright 2014 ACS Publication. d) Two-step ALD-CVD synthetic process and e) advantages and energy storage capability of $\text{TiS}_2@\text{CNTs}$ composite electrodes in Li^+ electrolyte.^[136] Reported with permission from ref 136. Copyright 2017 Wiley. f, g) SEM images of the core-shell $\text{Au}@ \text{MnO}_2$ NWs. h) Capacitance vs. scan rate for the $\text{Au}@ \text{MnO}_2$ NWs with various shell thicknesses as indicated.^[98] Reported with permission from ref 98. Copyright 2012 ACS Publication.

outstanding electrochemical stability with no capacitance decay in 10000 cycles. Lin reported the ALD method with the subsequent chemical vapor deposition (CVD) sulfurization to prepare the vertically aligned CNTs coated uniformly with the TiS_2 ^[136] as shown in Figure 12d. The high conductivity and large SSA of the vertically aligned CNTs framework improve the surface reactions and Li^+ ions intercalation into the core-shell $\text{TiS}_2@\text{CNTs}$ composite (Figure 12e). By optimizing the shell thickness, a high gravimetric SC of 195 F g^{-1} is obtained by the $\text{TiS}_2@\text{CNTs}$ composite, as well as excellent long-term stability with $>95\%$ of SC retention after 10000 cycles. Nickel and Au NWs have also been used as conductive cores to be coated with electroactive materials for elegant construction of 1D core-shell nano-architectures. Penner et al. demonstrated the fabrication of a mesoporous MnO_2 shell on top of Au NWs to form an Au core@ MnO_2 shell nanostructure (Figure 12f–g)^[98]. The core-shell Au@ MnO_2 NWs present a high SC of 1020 F g^{-1} at 5 mVs^{-1} . And the SCs of the hybrid NWs decrease with the

shell thickness increasing, owing to the increase in the ohmic drop with the shell thickness (Figure 12h).

Notably, PCMs often suffer from low electronic conductivity and poor cycling stability. Lots of studies confirm that the coating of conductive shell with good mechanical stability upon the electroactive core to form a core-shell nano-architecture can effectively address these issues.^[137,138] For example, Zhang and co-workers synthesized the reduced graphene oxide-wrapped MoO_3 NRs ($\text{rGO}@\text{MoO}_3$).^[139] Corresponding SEM and TEM observations (Figure 13a, b) reveal that the rGO phase uniformly covers on the surface of the MoO_3 core. The CV curves (Figure 13c) show the typical redox capacitive properties of the $\text{rGO}@\text{MoO}_3$. As a consequence, a high SC of 617 F g^{-1} is obtained at 1 Ag^{-1} , as well as good electrochemical stability with a SC retention of 87.5% after 6000 cycles. The rGO shell not only provides the increased electrical conductivity to facilitate the electron transfer but protects the MoO_3 core from collapsing during the charge-discharge process. As shown in Figure 13d, Liu et al. fabricated

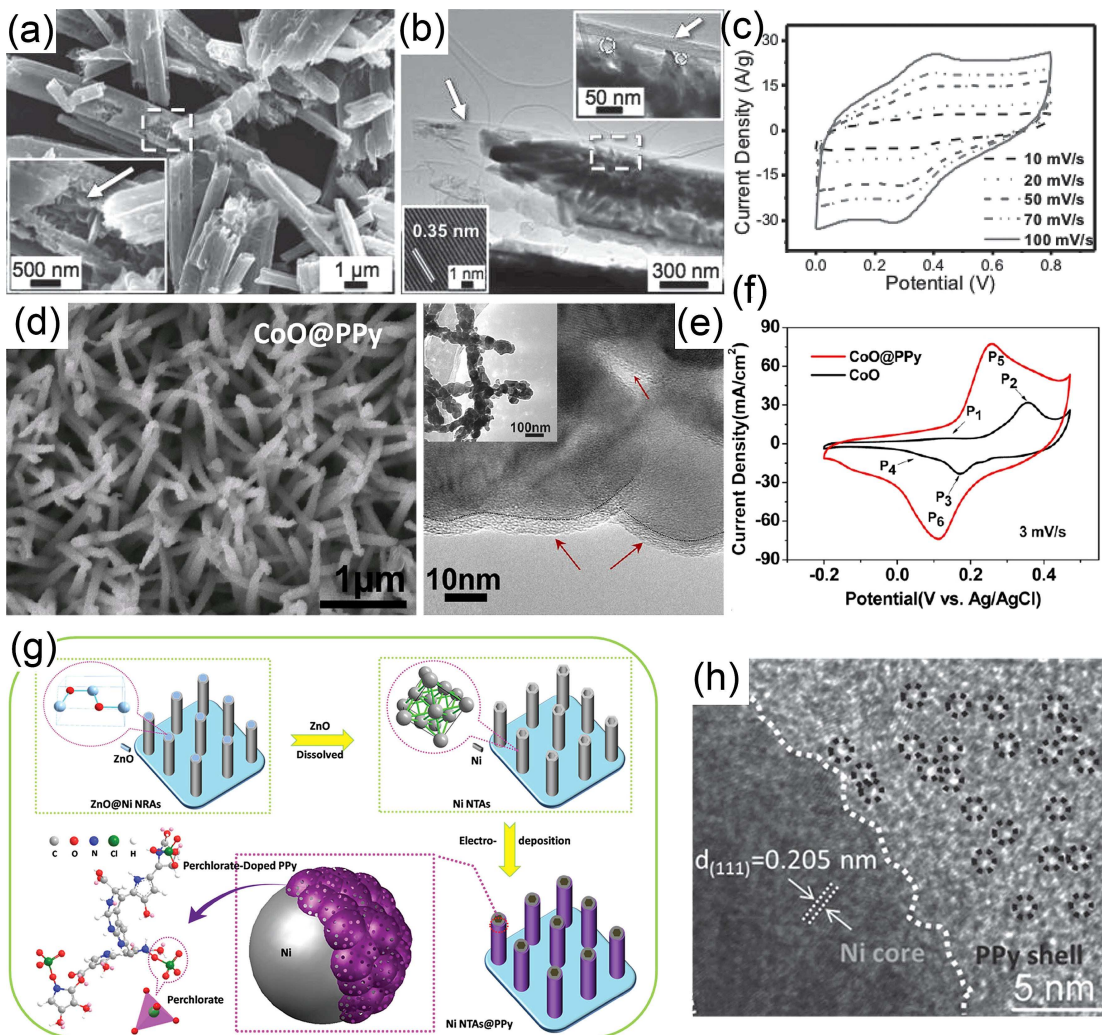


Figure 13. a) SEM, b) TEM images, and c) electrochemical performance of the rGO/ MoO_3 composite.^[139] Reported with permission from ref 139. Copyright 2015 Wiley. d) SEM and e) TEM images of the CoO@PPy NWs. f) CV curves of the optimized CoO@PPy and pristine CoO electrodes.^[140] Reported with permission from ref 140. Copyright 2013 ACS Publication. g) Schematic fabrication and h) HRTEM image of the NiNTAs@PPy.^[141] Reported with permission from ref 141. Copyright 2016 Wiley.

the core-shell CoO@PPy NW arrays on 3D nickel foam,^[140] where each CoO nanoparticle is shelled by a thin PPy layer (Figure 13e). It is due to the good conductivity of the PPy shell and short ion diffusion pathway in arrays that the CoO@PPy renders an ultrahigh SC of 2223 F g^{-1} (1338 C g^{-1}) and good rate performance, much higher than that of pristine CoO (Figure 13f). In addition, a series of 1D nanostructures are purposefully shelled with the conductive carbon or CPs coating shells with good mechanical stability to develop electrode materials for supercapacitors. Specifically, a core-shell nanoarray structure, i.e., the nickel NT arrays coated with porous perchlorate-doped PPy shell (NiNTAs@PPy) is developed,^[141] as schematic illustrated in Figure 13g. TEM observation (Figure 13h) reveals that the nickel NTs are densely coated by the PPy shell with abundant nanopores. More strikingly, the as-obtained NiNTAs@PPy can serve as both negative and positive electrodes with the impressive pseudocapacitive properties. Other core-shell composite systems like FeCo₂O₄@PPy NWs,^[142] PANI/sulfur-doped TiO₂ NT arrays,^[143] NiCo₂O₄@PPy NW arrays,^[144] tubular MoS₂/PANI,^[145] VO₂@PPy NW arrays,^[146] ZnO@CuS@PEDOT NR arrays decorated with MnO₂,^[147] and so on, are all promising electrodes for electrochemical supercapacitors.

Other core-shell NW arrays, where the pseudocapacitive metal oxides are both the core and shell materials, also have been investigated for supercapacitors. Fan et al. smartly fabricated a core-shell Co₃O₄@MnO₂ nanohybrid (Figure 14a, b).^[148] Benefiting from the ordered nano-arrays and synergistic contributions from electroactive Co₃O₄ core and MnO₂ shell, the Co₃O₄@MnO₂ composite exhibits excellent electrochemical capacitive properties (Figure 14c) in 1 M LiOH electrolyte. Furthermore, both the Faradaic reactions of Co³⁺/Co⁴⁺ associated

with OH⁻ ions and MnO₂ intercalated/deintercalated with Li⁺ ions contribute to the high SCs in aqueous LiOH solution. This work opens up a new strategy for design of PCMs without the conductive carbon or polymer media. The design concept has been extended to other various metal oxides. For instance, the sandwich-like MnO₂/Mn/MnO₂ NT arrays, as demonstrated in Figure 14d, are designed for supercapacitors.^[149] Such hybrid NT structure is endowed with convenient ion and electron pathways. The as-prepared MnO₂/Mn/MnO₂ electrode (Figure 14e) presents a large SC of 925 F g^{-1} at 5 mV s^{-1} , which is much higher than that of the pristine MnO₂ NT arrays (Figure 14f). Other cases, such as Zn₂SnO₄/MnO₂ nanocables,^[150] H-TiO₂//MnO₂//H-TiO₂@C NWS,^[151] Ni₃S₂@MoS₂ NR arrays,^[152] Ni(OH)₂@Fe₂O₃ NW arrays,^[153] Co₃O₄@NiCo₂O₄ NW arrays,^[154] CoMoO₄@CoNiO₂ NW arrays,^[155] NiCo₂O₄@MnO₂ NW arrays,^[156] and so on, have been further explored for supercapacitors. All of the hybrid core-shell architectures show superior electrochemical properties, which strongly highlights the fact that the electrochemical capacitance can be improved hugely by optimizing electroactive materials and specific nanostructures.

1D Subunits-Constructed Superstructures for Supercapacitors

1D nanostructured materials can work as the nano building blocks to consciously construct superstructures towards supercapacitors as high-performance electrodes, which combine geometrical advantages of both the subunits and high-level superstructures, and guarantee high-tap-density electrode materials for large volumetric SCs. Gao et al. prepared a Ni@NiO NW membrane through a simple filtration method.^[157] The

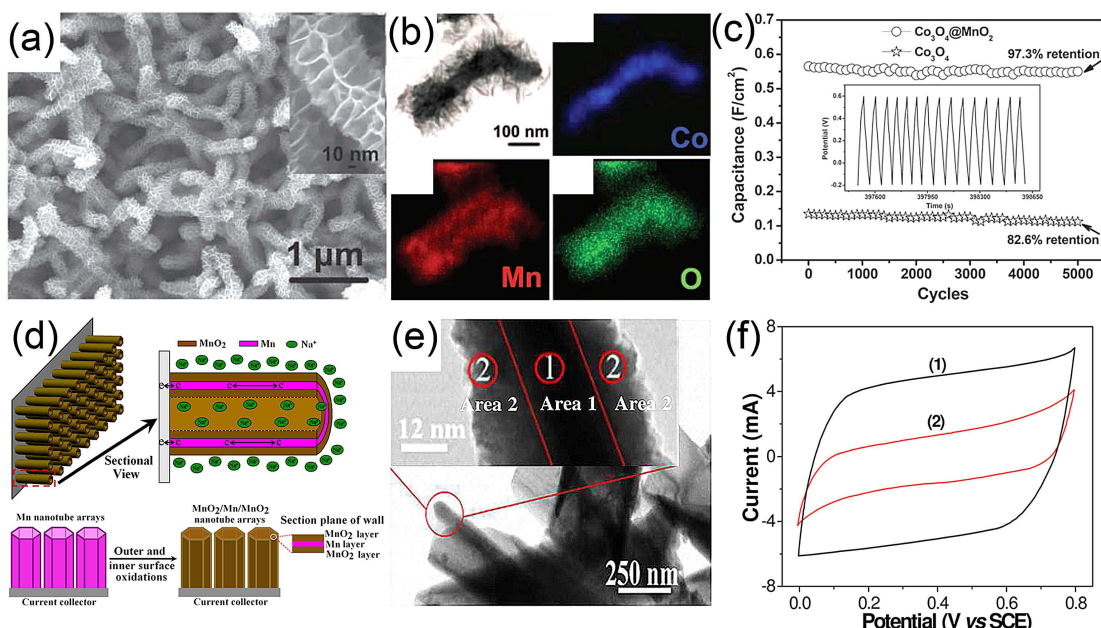


Figure 14. a) FESEM, b) TEM and EDS mapping of the Co₃O₄@MnO₂ core-shell NWs. c) Cycling performance of both the Co₃O₄@MnO₂ and pristine Co₃O₄ arrays (inset is the charge-discharge curves of the last 15 cycles for Co₃O₄@MnO₂).^[148] Reported with permission from ref 148. Copyright 2011 Wiley. d) Novel structures provide fast pathways for ions/electrons and fabricate illustration of MnO₂/Mn/MnO₂ hybrid nanostructures. e) TEM image of MnO₂/Mn/MnO₂ NTs. f) CV curves of (1) MnO₂/Mn/MnO₂ and (2) pristine MnO₂ NTs at a scan rate of 5 mV s^{-1} .^[149] Reported with permission from ref 149. Copyright 2012 ACS Publication.

membrane constructed by ultralong Ni NWs (Figure 15 a, b) shows a thickness of 26 μm and good flexibility with no obvious mechanical damage under bending conditions (Figure 15c). The unique hierarchical structure not only facilitates the ions transport velocity but provides Faradaic capacitance contribution. Thus, the flexible electrode preserves a high gravimetric SC of 530 Fg^{-1} (265 Cg^{-1}), i.e., 38.4 Fcm^{-3} (19.2 Ccm^{-3}) at 0.032 Acm^{-3} , and good rate capability. 1D

nanostructured PCMs also have been integrated with CNTs to fabricate free-standing membrane electrodes, such as V_2O_5 /CNTs composite,^[67] MnO_2 NFs/CNTs hybrid film,^[158] and $\text{CoSeO}_3\text{-H}_2\text{O}$ nanoribbon/CNTs composite paper,^[159] for the flexible and self-supporting supercapacitors. Recently, a 3D sea-urchin-like $\text{Ni}_{0.5}\text{Co}_{0.5}\text{Se}_2$ specimen constructed by 1D porous NWs is synthesized, as illustrated in Figure 15d.^[160] The unique 3D architecture with porous NWs blocks (Figure 15e) provides a

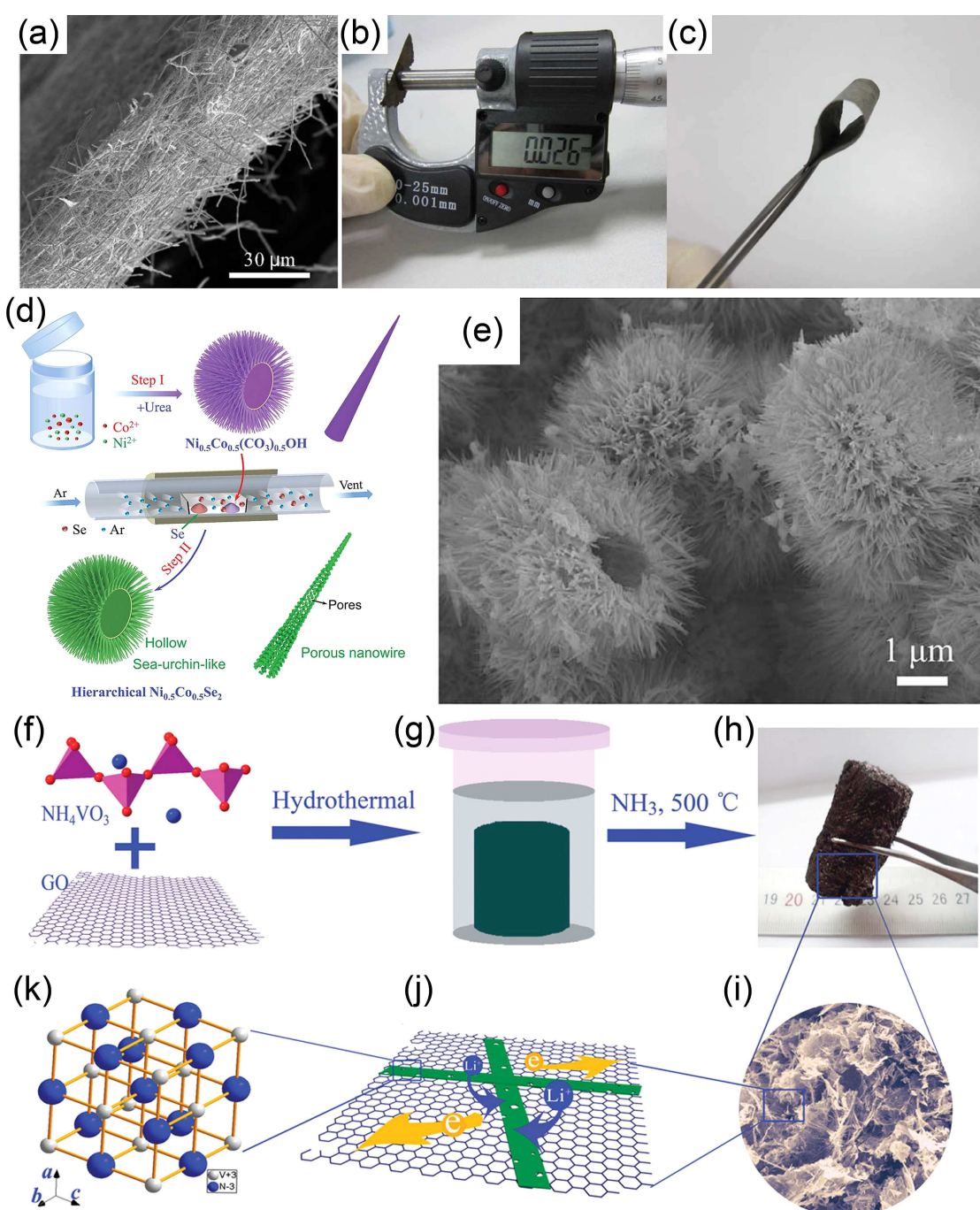


Figure 15. a) Cross-sectional FESEM image of free-standing Ni@NiO NW membrane. b), c) Digital images of the free-standing Ni@NiO membrane with a thickness of 26 μm and high flexibility.^[157] Reported with permission from ref 157. Copyright 2014 ACS Publication. d) FESEM image of the 3D sea-urchin-like $\text{Ni}_{0.5}\text{Co}_{0.5}\text{Se}_2$.^[160] Reported with permission from ref 160. Copyright 2018 RSC Publication. f), g) Schematic fabrication, h) digital graph, and i) FESEM image of the 3D porous VN-RGO composite. j) Schematic of intimate contacts between VN and graphene facilitating the charge transport and Li^+ intercalation. k) VN crystal structure.^[165] Reported with permission from ref 165. Copyright 2015 Wiley.

plenty of electro-active sites and sufficient electrode/electrolyte contacting sur-/interfaces. As a result, the $\text{Ni}_{0.5}\text{Co}_{0.5}\text{Se}_2$ electrode renders superior capacitance and good cycling stability. Up till now, a variety of 3D hierarchical structures from 1D nano-subunits have been developed, such as dandelion-like molybdenum-nickel-cobalt ternary oxide,^[161] hierarchical $\text{Ni}_{0.3}\text{Co}_{2.7}\text{O}_4$ architecture,^[162] urchin-like NiCo_2O_4 microspheres,^[163] urchin-like ordered $\text{Co}(\text{OH})_2$ arrays,^[164] hierarchical porous network-like NiCo_2O_4 framework,^[165] and so on. These 3D hierarchical superstructures often hold high SSA and effectively prevent the aggregation of the primary nanostructures, which is favorable for convenient ionic diffusion and electronic transport in high-rate charge storage.

Furthermore, 1D nano blocks have also been utilized to construct 3D structures by using the graphene as the assisted component. For example, 3D graphene/PPy aerogel is fabricated with the graphene and PPy NTs as the building blocks for supercapacitors.^[166] A typical synergistic effect is observed on the graphene/PPy aerogel. More specifically, the well-defined PPy NTs work as pillars to prevent the restacking of graphene sheets, thus providing a large accessible surface for fast transport of H^+ ions, while the interconnected graphene act as the continuous current collector to facilitate the electron transfer. The interesting design can be extended to 1D metal oxides/nitrides nanostructures. Recently, Yan and co-workers fabricated a 3D porous VN NWs-graphene composite (Figure 15f-h) as an anode for high-performance Li-ion supercapacitors.^[167] The complementary combination of 1D VN NWs and graphene ensures the fast charge transport and Li intercalation (Figure 15i-k), and makes the VN-rGO based hybrid supercapacitor an energy density of 162 Wh kg^{-1} at 200 W kg^{-1} . Huang et al. reported that the synthesis of 3D

hierarchical composite with 1D $\text{Zn}_{0.25}\text{V}_2\text{O}_5\text{nH}_2\text{O}$ (ZVO) NBs and rGO sheets. The layered structure ZVO is spacious enough to facilitate the fast Na^+ insertion/extraction without severe volume change, which renders the predominantly pseudocapacitive behaviors during the charge storage process, while 3D rGO backbone is in favor of electron movement through the formation of a continuously conducting network. Thus, the outstanding rate capability and long-life characteristic of the ZVO/rGO are observed in half-cell evaluation.^[168]

Defect Engineering Strategies in 1D PCMs for Supercapacitors

Besides the structural/componential optimizations, compositional design plays an equal role in enhancing electrochemical properties of the 1D PCMs for supercapacitors. Recently, the defect engineering strategies such as oxygen vacancies and heteroatom-doping have been explored to improve intrinsic conductivities and electrochemical activities of the PCMs for even better supercapacitive behaviors. The defects in crystal structure can change the geometric and electronic structure of the active materials themselves, and thus their electrochemical properties.^[106,169,170] Dunn et al. reported the introduction of oxygen vacancies into the nanobelt-like $\alpha\text{-MoO}_3$ to substantially improve its capacitive behaviors (Figure 16a, b). The presence of oxygen vacancies provides better electrical conductivity and expanded interlayer space, which can promote the kinetics and preserve the $\alpha\text{-MoO}_3$ structure during Li^+ insertion/desertion processes. The *ex-situ* XPS demonstrates that the formation of the Mo^{4+} during the reversibly lithiation process in the oxygen-deficient MoO_{3-x} may account for its high

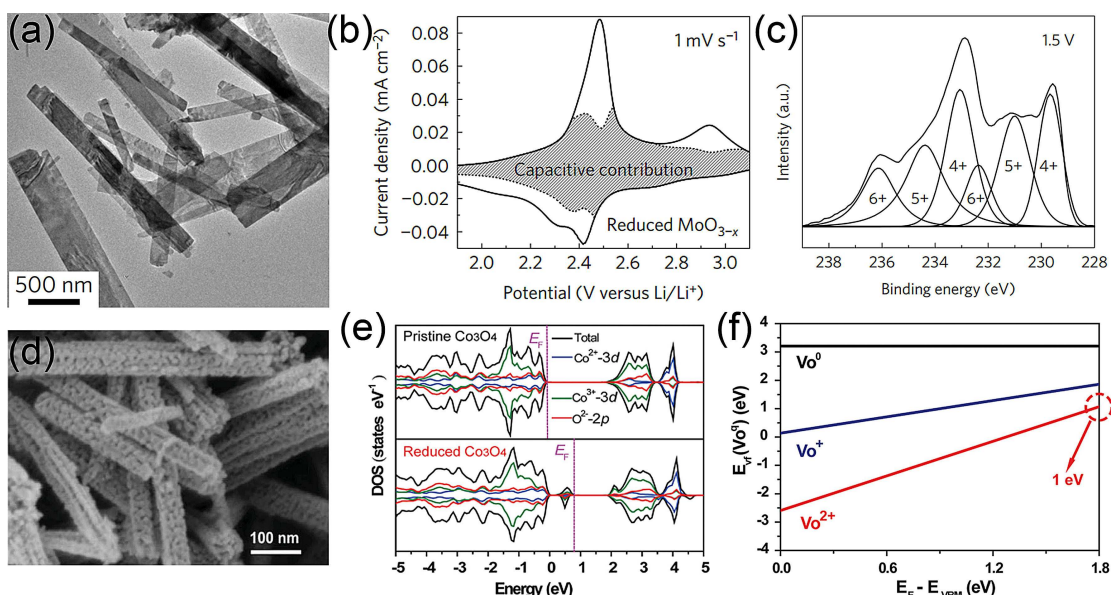


Figure 16. a) TEM image of oxygen-deficient MoO_{3-x} . b) Voltammetry measurements show that MoO_{3-x} exhibits pseudocapacitive charge storage properties. c) Ex-situ XPS of the Mo 3d region in MoO_{3-x} at the lithiated state.^[171] Reported with permission from ref 171. Copyright 2017 Nature Publishing Group. d) SEM image of the reduced Co_3O_4 NWs. e) DOSs of the pristine Co_3O_4 and the reduced Co_3O_4 (with oxygen vacancies). f) Calculated formation energy for the reduced Co_3O_4 . Vo^{2+} , Vo^+ , Vo^0 denote the gap state is empty, occupied by one and two electrons, respectively.^[172] Reported with permission from ref 172. Copyright 2014 Wiley.

SCs (Figure 16c).^[171] Additionally, Zheng and co-authors demonstrate the introduction of oxygen vacancies in mesoporous Co_3O_4 NWs (Figure 16d) through a chemical reduction method.^[172] A three-fold increase in SC values is observed, which can be attributed to the enhanced conductivity and superior electrochemical activity of oxygen vacancy defected Co_3O_4 . Density functional theory calculations indicate that new defect states are generated by the oxygen vacancies and the calculated formation energy reveals that two electrons on the oxygen vacancy defect can be easily excited into the conduction band, thus resulting in an improved electrical conductivity of the Co_3O_4 itself (Figure 16e–f). For other cases, such as oxygen-deficient MnO_2 NRs by hydrogenation treatment, core-shell Ti-doped $\text{Fe}_2\text{O}_3@\text{PEDOT}$ NRs, sulfur-doped $\text{V}_6\text{O}_{13-x}$, and oxygen-deficient hematite NRs for pseudo-supercapacitors are also extensively studied.^[124,173–175] Overall, these constructive works demonstrate the potential importance of incorporating defects or vacancies into 1D PCMs as an effective strategy for increasing the charge-storage capacity and kinetics of the redox-active materials.

Outlook and Challenges

In the review, we have summarized the recent research progress in rational design and controllable synthesis of 1D nanostructured PCMs and their promising applications for high-performance supercapacitors, besides the in-depth understanding of pseudocapacitive mechanisms. The intrinsically electrochemical and geometrical merits including large Faradaic SCs and remarkable ions/electrons transport in electrodes endow the 1D nanostructured PCMs with anticipatively high energy densities but not at the expense of their rate behaviors, along with the fine structural, componential and compositional manipulations via purposefully synthetic optimizations. As discussed above, various 1D conventional nanostructures (i.e., NRs, NBs, NFs, NTs, etc.), nano-arrays, core-shell nano-architectures 1D subunits-built superstructures, and defect engineering strategies in 1D PCMs are extensively explored with the aim to boost their electrochemical behaviors and promote their practical applications in advanced supercapacitors. And a brief summary of the 1D nanostructured PCMs as electrodes towards high-performance supercapacitors are comparatively given in Table 1. Encouragingly, 1D nanostructured PCMs generally possess significant advantages for developing supercapacitor devices compared to their bulk counterparts and/or other nanostructured forms. Nevertheless, to maximize the full potential applications of 1D nanostructured PCMs, some critical aspects still require systematically exploration:

First, the majority of the reported synthetic strategies of 1D nanostructured PCMs are mainly limited to the laboratory research, and somewhat difficult for industrial production. In the coming decades, it is more compelling to develop simple, scalable, cost-effective yet high-repetition-rate synthesis approaches for efficient fabrication of high-quality 1D PCMs with desired electrochemical performance for supercapacitors.

Second, the thorough and in-depth understanding of generation and fading mechanism of pseudocapacitance is an everlasting topic in the field of electrochemical supercapacitors, and hold the key to fully optimize their ultimate electrochemical performances. Systematical investigations based on the smart combination of *in-situ* spectroscopic techniques (such as, TEM, X-ray diffraction, Raman, nuclear magnetic resonance, electrochemical quartz crystal microbalance, electrochemical atomic force microscope, etc.) and theoretical simulation/calculation would be cogent methodologies to shed light upon the more complex charge-storage mechanisms in supercapacitors, and establish a fundamental and intrinsic relationship between electrochemical charge/mass transfer and unique 1D nano-dimensional microstructures (diameter, aspect ratio, pore structure, crystalline structure, surface physiochemical properties, etc.), which can be further used as the guidance for purposeful design of 1D PCMs electrodes. Although 1D nanostructured materials are favorable research model for theoretically and experimentally to reveal the aforementioned scientific issues, unfortunately, related studies in supercapacitors has been seriously limited so far.

Third, micro-/nanoscale supercapacitors, such as conventional sandwich-like and interdigitated micro-supercapacitors, are becoming attractive for the new development of on chip device systems due to their large areal/volumetric SCs and high energy/power density compared to the traditional capacitors. Nonetheless, the proper yet effective design of micro-electrodes with outstanding supercapacitive properties and manufacture techniques still need to be improved to meet the increased requirements of micro electrical smart devices. The intrinsic advantages of 1D nanostructured materials provide the possibility for them to develop the required micro/nano-scale supercapacitors with more versatile functions including fast-frequency response, flexibility, wear-ability and transparency. Thus, it can be highly predictable that more and more novel yet high-performance micro-/nanoscale supercapacitors even with several special features would be elegantly constructed with the rapid development of these promising 1D nanostructured PCMs

Last but not the least, except for the electrode and device optimization, the involved electrolytes also play a significant role in enhancing the electrode kinetics, even at low operating temperatures for better electrochemical properties.^[194–197] Specifically, the introduction of highly reversible ion pairs (such as $\text{Fe}(\text{CN})_6^{3-}/\text{Fe}(\text{CN})_6^{4-}$, p -phenylenediamine/ p -benzoquinone, etc.) in electrolytes, as the “electron relay” at the electrode/electrolyte interfaces during charge-discharge process by coupling in the redox reaction in the PCMs, would decrease charge-transfer resistance and increase exchange current density, favoring for the improvement in electrochemical capacitances. Therefore, the smart integration of appropriate redox-mediated electrolytes with these optimized 1D pseudocapacitive electrodes and corresponding micro-/nanoscale devices would be another appealing way to fabricate supercapacitors with excellent electrochemical properties. Moreover, the underlying interacting mechanisms between 1D PCMs and various redox-

Table 1. Summary of electrochemical performance of the representative 1D nanostructured PCMs with different electrolytes.

Structures	Materials	Electrolytes	SCs	Cycling stabilities	Ref.
1D nano-arrays	MnO ₂ NWs	1 M LiClO ₄	923 F g ⁻¹ , 5 mVs ⁻¹	90%, 5000 cycles	110
	NiCo ₂ O ₄ NWs	6 M KOH	401 F g ⁻¹ (~180.45 Cg ⁻¹), 1 Ag ⁻¹	98%, 2000 cycles	111
	Co ₃ O ₄ NWs	2 M KOH	260 F g ⁻¹ (~130 Cg ⁻¹), 2 Ag ⁻¹	95%, 5000 cycles	22
	Cu ₇ S ₄ NWs		400 F g ⁻¹ , 10 mVs ⁻¹	74%, 3000 cycles	176
	MoO ₃ NRs	1 M H ₂ SO ₄	230 F g ⁻¹ , 0.25 Ag ⁻¹	95%, 500 cycles	177
	α -MoO ₃ NBs	0.5 M Li ₂ SO ₄	369 F g ⁻¹ , 0.1 Ag ⁻¹	95%, 500 cycles	25
	PANI NTs	EMIMBF ₄	152 F g ⁻¹ , 1 Ag ⁻¹	95.3%, 5000 cycles	24
	Fe ³⁺ doped MnO ₂ NWs	0.5 M Na ₂ SO ₄	243 F g ⁻¹ , 1 Ag ⁻¹	86%, 1000 cycles	112
	Mesoporous α -Ni(OH) ₂ NWs		2223 F g ⁻¹ , 1 Ag ⁻¹	90%, 3000 cycles	178
	Co ₂ P ₂ O ₇ NRs	3 M KOH	483 F g ⁻¹ (~265.65 Cg ⁻¹), 1 Ag ⁻¹	90.4%, 4700 cycles	115
	Li ₃ VO ₄ /N-doped carbon NWs	LiPF ₆	372 mAhg ⁻¹ , 1 Ag ⁻¹	88%, 1500 cycles	48
	PANI NW arrays	1 M HClO ₄	950 F g ⁻¹ , 1 Ag ⁻¹	78%, 500 cycles	121
1D core-shell nano-architectures	TiC tubular arrays	1.5 M LiClO ₄ in acetonitrile	185 F g ⁻¹ , 2 Ag ⁻¹	97%, 150000 cycles	179
	NiCo ₂ O ₄ nanoneedle arrays		3.12 F cm ⁻² (~1.25 C cm ⁻²), 1.11 mAcm ⁻²	89.4%, 2000 cycles	180
	TiN NT arrays	1 M KOH	167 F g ⁻¹ , 1 Ag ⁻¹	70%, 6000 cycles	181
	NiCo ₂ O ₄ tetragonal microtubes		1387.9 F g ⁻¹ (~735.6 Cg ⁻¹), 2 Ag ⁻¹	89.4%, 12000 cycles	182
	WON NW arrays		4.95 F cm ⁻³ , 12.5 mAcm ⁻³	93%, 100000 cycles	127
	TiO ₂ NT arrays	0.5 M Na ₂ SO ₄	1.84 mFcm ⁻² , 5 mVs ⁻¹	93.1%, 2000 cycles	103
	F-doped β -FeOOH NR arrays		1094.74 F g ⁻¹ (1.12 F cm ⁻²), 1 mAcm ⁻²	~100%, 5000 cycles	183
	Co ₃ O ₄ NW arrays	6 M KOH	1160 F g ⁻¹ (~580 Cg ⁻¹), 2 Ag ⁻¹	90.4%, 4700 cycles	184
	RuO ₂ NT arrays	1 M H ₂ SO ₄	1300 F g ⁻¹ , 10 mVs ⁻¹	97%, 1800 cycles	120
	Core-shell CNTs@V ₂ O ₅	1 M LiClO ₄ in 1:1 ethylene carbonate and dimethyl carbonate	2780 Cg ⁻¹ , 0.1 mVs ⁻¹	96.3%, 10000 cycles	185
	Core-shell rGO@MoO ₃	1 M H ₂ SO ₄	617 F g ⁻¹ , 1 Ag ⁻¹	87.5%, 2000 cycles	139
	Core-shell CoO@PPy		2223 F g ⁻¹ , 1 mAcm ⁻²	99.8%, 2000 cycles	140
1D materials constructed superstructures	Core-shell CNTs@NiCo ₂ O ₄	2 M KOH	1472 F g ⁻¹ (~809.6 Cg ⁻¹), 1 Ag ⁻¹	99%, 3000 cycles	186
	Core-shell Ni/NiO	1 M KOH	1635 F g ⁻¹ (~981 Cg ⁻¹), 2 mVs ⁻¹	94.8%, 1200 cycles	187
	Core-shell ZnCo ₂ O ₄ @MnO ₂	1 M KOH	1981 F g ⁻¹ (~990.5 Cg ⁻¹), 5 Ag ⁻¹	90%, 2000 cycles	188
	Core-shell ZnO@MnO ₂	1 M Na ₂ SO ₄	405 F g ⁻¹ , 10 mVs ⁻¹	95.1%, 6000 cycles	189
	Core-shell WO _{3-y} @Au@MnO ₂	0.1 M Na ₂ SO ₄	588 F g ⁻¹ , 10 mV ⁻¹	100%, 5000 cycles	28
	Core-shell Co ₃ O ₄ @NiO	2 M KOH	853 F g ⁻¹ (~469 Cg ⁻¹), 2 A g ⁻¹	91%, 3500 cycles	190
	Core-shell Ni ₃ S ₂ @MoS ₂	2 M KOH	848 F g ⁻¹ , 5 Ag ⁻¹	97%, 1800 cycles	153
	2D MnO ₂ NW network	1 M Na ₂ SO ₄	453 F g ⁻¹ , 0.5 Ag ⁻¹	95%, 10000 cycles	191
	2D VN/CNT complex structure	0.5 M Na ₂ SO ₄	178 mFcm ⁻² , 1.1 mAcm ⁻²	95%, 3000 cycles	192
	2D MnO ₂ /CNT hybrid structure	5 M LiCl	508 mFcm ⁻² , 1.6 mAcm ⁻²	98.1%, 2000 cycles	106
	NRs-constructed 3D Ni _{0.3} Co _{2.7} O ₄	3 M KOH	960 F g ⁻¹ (~432 Cg ⁻¹), 0.625 Ag ⁻¹	91%, 2000 cycles	162
	Urchin-like Ni _{0.5} Co _{0.5} Se ₂	6 M KOH	524 F g ⁻¹ , 1 Ag ⁻¹	90%, 2000 cycles	160
	3D VN NWs-rGO hydrogel	1 M LiPF ₆	470 mAhg ⁻¹ , 1 Ag ⁻¹	96.3%, 10000 cycles	167
	3D MnO ₂ NBs-rGO hydrogel	6 M KOH	362 F g ⁻¹ , 1 Ag ⁻¹	93%, 10000 cycles	193

mediated electrolytes will be reasonably clarified with comprehensive investigation in this field.

Overall, there is still enormous room left in further design and fine synthesis of 1D nanoscaled PCMs with competitive supercapacitances towards next-generation supercapacitors, although fruitful achievements have been obtained till now. Appealingly, we strongly believe that any further breakthrough in such field will stimulate the rapid development of 1D PCMs-based supercapacitors with high energy/power density and superior long-duration cycling stabilities with the close collaboration between electrochemists, chemists and theoreticians in the near future, despite of the daunting challenges ahead.

Acknowledgements

The authors acknowledge the financial support from National Natural Science Foundation of China (No. 51772127, 51772131, 41800347), Taishan Scholars (No. ts201712050), Major Program of Shandong Province Natural Science Foundation (ZR2018ZB0317)

and Collaborative Innovation Center of Technology and Equipment for Biological Diagnosis and Therapy in Universities of Shandong.

Conflict of interest

The authors declare no conflict of interest.

Keywords: one-dimensional nanostructures · pseudocapacitive materials · Faradaic mechanisms · supercapacitors

- [1] C. Zhong, Y. Deng, W. Hu, J. Qiao, L. Zhang, J. Zhang, *Chem. Soc. Rev.* **2015**, *44*, 7484–7539.
- [2] P. Simon, Y. Gogotsi, *Nat. Mater.* **2008**, *7*, 845–854.
- [3] B. E. Conway, Electrochemical supercapacitors: scientific fundamentals and technological applications, *Kluwer Academic*, **1999**.
- [4] Y. Shao, M. F. El-Kady, J. Sun, Y. Li, Q. Zhang, M. Zhu, H. Wang, B. Dunn, R. B. Kaner, *Chem. Rev.* **2018**, *118*, 9233–9280.
- [5] J. Yan, Q. Wang, T. Wei, Z. Fan, *Adv. Energy Mater.* **2014**, *4*, 1300816.

- [6] J. W. Long, D. Bélanger, T. Brousse, W. Sugimoto, M. B. Sassin, O. Crosnier, *MRS Bull.* **2011**, *36*, 513–522.
- [7] M. Watanabe, M. L. Thomas, S. Zhang, K. Ueno, T. Yasuda, K. Dokko, *Chem. Rev.* **2017**, *117*, 71907239.
- [8] J. Wang, S. Dong, B. Ding, Y. Wang, X. Hao, H. Dou, Y. Xia, X. Zhang, *Natl. Sci. Rev.* **2017**, *4*, 71–90.
- [9] J. F. Sun, C. Wu, X. F. Sun, H. Hu, C. Y. Zhi, L. R. Hou, C. Z. Yuan, *J. Mater. Chem. A* **2017**, *5*, 94439464.
- [10] F. Wang, X. Wu, X. Yuan, Z. Liu, Y. Zhang, L. Fu, Y. Zhu, Q. Zhou, Y. Wu, W. Huang, *Chem. Soc. Rev.* **2017**, *46*, 6816–6854.
- [11] K. P. Annamalai, X. Zheng, J. Gao, T. Chen, Y. Tao, *Carbon* **2019**, *144*, 185–192.
- [12] W. Fu, E. Zhao, X. Ren, A. Magasinski, G. Yushin, *Adv. Energy Mater.* **2018**, *8*, 1703454.
- [13] M. Acerce, D. Voiry, M. Chhowalla, *Nat. Nanotechnol.* **2015**, *10*, 313–318.
- [14] Y. Yi, L. Yu, Z. Tian, Y. Song, Y. Shao, L. Gao, J. Sun, Z. Liu, *Adv. Funct. Mater.* **2018**, *28*, 1805510.
- [15] L. R. Hou, Y. Y. Shi, C. Wu, Y. R. Zhang, Y. Z. Ma, X. Sun, J. F. Sun, X. G. Zhang, C. Z. Yuan, *Adv. Funct. Mater.* **2018**, *13*, 1705921.
- [16] K. Wang, H. Wu, Y. Meng, Z. Wei, *Small* **2014**, *10*, 14–31.
- [17] H. B. Wu, G. Q. Zhang, L. Yu, X. W. Lou, *Nanoscale Horiz.* **2016**, *1*, 27–40.
- [18] Q. Wei, F. Xiong, S. Tan, L. Huang, E. H. Lan, B. Dunn, L. Mai, *Adv. Mater.* **2017**, *29*, 1602300.
- [19] J. N. Tiwari, R. N. Tiwari, K. S. Kim, *Prog. Mater. Sci.* **2012**, *57*, 724–803.
- [20] C. Z. Yuan, H. B. Wu, Y. Xie, X. W. Lou, *Angew. Chem. Int. Ed.* **2014**, *5*, 1488–1504.
- [21] X. Ma, W. Luo, M. Yan, L. He, L. Mai, *Nano Energy* **2016**, *24*, 165–188.
- [22] B. Wang, T. Zhu, H. B. Wu, R. Xu, J. S. Chen, X. W. Lou, *Nanoscale* **2012**, *4*, 2145–2149.
- [23] C. Chen, S. Wang, X. Luo, W. Gao, G. Huang, Y. Zeng, Z. Zhu, *J. Power Sources* **2019**, *409*, 112–122.
- [24] W. Chen, R. B. Rakhi, H. N. Alshareef, *J. Mater. Chem. A* **2013**, *1*, 3315–3324.
- [25] J. Jiang, J. Liu, S. Peng, D. Qian, D. Luo, Q. Wang, Z. Tian, Y. Liu, *J. Mater. Chem. A* **2013**, *1*, 2588–2594.
- [26] D. Guo, L. Lai, A. Cao, H. Liu, S. Dou, J. Ma, *RSC Adv.* **2015**, *5*, 55856–55869.
- [27] S. M. Mirvakili, I. W. Hunter, *Adv. Mater.* **2017**, *29*, 1700671.
- [28] X. Lu, T. Zhai, X. Zhang, Y. Shen, L. Yuan, B. Hu, L. Gong, J. Chen, Y. Gao, J. Zhou, Y. Tong, Z. L. Wang, *Adv. Mater.* **2012**, *24*, 938–944.
- [29] B. Yao, L. Huang, J. Zhang, X. Gao, J. Wu, Y. Cheng, X. Xiao, B. Wang, Y. Li, J. Zhou, *Adv. Mater.* **2016**, *28*, 6353–6358.
- [30] Y. Jiang, L. Jiang, Z. Wu, P. Yang, H. Zhang, Z. Pan, L. Hu, *J. Mater. Chem. A* **2018**, *6*, 16308–16315.
- [31] L. Mai, X. Tian, X. Xu, L. Chang, L. Xu, *Chem. Rev.* **2014**, *114*, 11828–11862.
- [32] R. S. Devan, R. A. Patil, J.-H. Lin, Y.-R. Ma, *Adv. Funct. Mater.* **2012**, *22*, 3326–3370.
- [33] D. Zhao, Y. Wang, Y. Zhang, *Nano-Micro Lett.* **2011**, *3*, 62–71.
- [34] J. Xie, C. Guo, C. Li, *Energy Environ. Sci.* **2014**, *7*, 2559–2579.
- [35] Q. Yang, Z. Lu, T. Li, X. Sun, J. Liu, *Nano Energy* **2014**, *7*, 170–178.
- [36] V. Augustyn, P. Simon, B. Dunn, *Energy Environ. Sci.* **2014**, *7*, 1597–1614.
- [37] Q. Jiang, N. Kurra, M. Alhabeb, Y. Gogotsi, H. N. Alshareef, *Adv. Energy Mater.* **2018**, *8*, 1703043.
- [38] P. Simon, Y. Gogotsi, B. Dunn, *Science* **2014**, *343*, 1210–1211.
- [39] T. Brousse, D. Belanger, J. W. Long, *J. Electrochem. Soc.* **2015**, *162*, A5185–A5189.
- [40] A. Eftekhari, M. Mohamedi, *Mater. Today Energy* **2017**, *6*, 211–229.
- [41] V. Sudha, M. V. Sangaranarayanan, *J. Phys. Chem. B* **2002**, *106*, 2699–2707.
- [42] E. Herrero, L. J. Buller, H. D. Abruna, *Chem. Rev.* **2001**, *101*, 1897–1930.
- [43] V. Augustyn, J. Come, M. A. Lowe, J. W. Kim, P.-L. Taberna, S. H. Tolbert, H. D. Abruna, P. Simon, B. Dunn, *Nat. Mater.* **2013**, *12*, 518–522.
- [44] H. Li, Y. Zhu, S. Dong, L. Shen, Z. Chen, X. Zhang, G. Yu, *Chem. Mater.* **2016**, *28*, 5753–5760.
- [45] X. Wang, G. Shen, *Nano Energy* **2015**, *15*, 104–115.
- [46] Z. Chen, V. Augustyn, J. Wen, Y. Zhang, M. Shen, B. Dunn, Y. Lu, *Adv. Mater.* **2011**, *23*, 791–795.
- [47] R. Wang, S. Wang, X. Peng, Y. Zhang, D. Jin, P. K. Chu, L. Zhang, *ACS Appl. Mater. Interfaces* **2017**, *9*, 32745–32755.
- [48] L. Shen, H. Lv, S. Chen, P. Kopold, P. A. van Aken, X. Wu, J. Maier, Y. Yu, *Adv. Mater.* **2017**, *29*, 1700142.
- [49] S. Wang, R. Wang, Y. Bian, D. Jin, Y. Zhang, L. Zhang, *Nano Energy* **2019**, *55*, 173–181.
- [50] X. Wang, S. Kajiyama, H. Iinuma, E. Hosono, S. Oro, I. Moriguchi, M. Okubo, A. Yamada, *Nat. Commun.* **2014**, *6*, 6544.
- [51] Y. Wang, Y. Song, Y. Yao, *Chem. Soc. Rev.* **2016**, *45*, 5925–5950.
- [52] M. R. Lukatskaya, B. Dunn, Y. Gogotsi, *Nat. Commun.* **2016**, *7*, 12647.
- [53] M. Okubo, E. Hosono, J. Kim, M. Enomoto, N. Kojima, T. Kudo, H. Zhou, I. Honma, *J. Am. Chem. Soc.* **2007**, *129*, 7444–7452.
- [54] T. Wang, H. C. Chen, F. Yu, X. S. Zhao, H. Wang, *Energy Storage Mater.* **2019**, *16*, 545–573.
- [55] S. Cheng, L. Yang, D. Chen, X. Ji, Z. Jiang, D. Ding, M. Liu, *Nano Energy* **2014**, *9*, 161–167.
- [56] D. Chen, X. Xiong, B. Zhao, M. A. Mahmoud, M. A. El-Sayed, M. Liu, *Adv. Sci.* **2016**, *3*, 1500433.
- [57] T. Brezesinski, J. Wang, S. H. Tolbert, B. Dunn, *Nat. Mater.* **2010**, *9*, 146–151.
- [58] S. H. Ko, D. Le, H. W. Kang, K. H. Nam, J. Y. Yeo, S. J. Hong, *Nano Lett.* **2011**, *11*, 666–671.
- [59] J. Qu, G. R. Li, X. P. Gao, *Energy Environ. Sci.* **2010**, *3*, 2003–2009.
- [60] E. Hosono, T. Saito, J. Hoshino, M. Okubo, Y. Saito, D. Nishio-Hamane, T. Kudo, H. Zhou, *J. Power Sources* **2012**, *217*, 43–46.
- [61] Z. Yu, L. Tetard, L. Zhai, J. Thomas, *Energy Environ. Sci.* **2015**, *8*, 702–730.
- [62] H. M. Chen, C. K. Chen, R.-S. Liu, L. Zhang, J. Zhang, D. P. Wilkinson, *Chem. Soc. Rev.* **2012**, *41*, 5654–5671.
- [63] Y. Wang, Y. Wang, D. Jia, Z. Peng, Y. Xia, G. Zheng, *Nano Lett.* **2014**, *14*, 1080–1084.
- [64] Y. Wang, J. Zeng, J. Li, X. Cui, A. M. Al-Enizi, L. Zhang, G. Zheng, *J. Mater. Chem. A* **2015**, *3*, 1638216392.
- [65] K. Wang, Q. Meng, Y. Zhang, Z. Wei, M. Miao, *Adv. Mater.* **2013**, *25*, 1494–1498.
- [66] M. Ge, C. Cao, J. Huang, S. Li, Z. Chen, K.-Q. Zhang, S. S. Al-Deyab, Y. Lai, *J. Mater. Chem. A* **2016**, *4*, 6772–6801.
- [67] X. Wang, Z. Li, J. Shi, Y. Yu, *Chem. Rev.* **2014**, *114*, 9346–9384.
- [68] S. Liu, C. Mao, Yubin Niu, F. Yi, J. Hou, S. Lu, J. Jiang, M. Xu, C. Li, *ACS Appl. Mater. Interfaces* **2015**, *7*, 25568–25573.
- [69] F. Jiang, A. J. Muscat, *Langmuir* **2012**, *28*, 12931–12940.
- [70] M. Igglund, M. Mazzotti, *Cryst. Growth Des.* **2012**, *12*, 1489–1500.
- [71] P. Yang, Y. Ding, Z. Lin, Z. Chen, Y. Li, P. Qiang, M. Ebrahimi, W. Mai, C. P. Wong, Z. L. Wang, *Nano Lett.* **2014**, *14*, 731–736.
- [72] Z. Chen, V. Augustyn, X. Jia, Q. Xiao, B. Dunn, Y. Lu, *ACS Nano* **2012**, *6*, 4319–4327.
- [73] H. Jiang, J. J. Hong, X. Wu, T. W. Surta, Y. Qi, S. Dong, Z. Li, D. P. Leonard, J. J. Holoubek, J. C. Wong, J. J. Razink, X. Zhang, X. Ji, *J. Am. Chem. Soc.* **2018**, *140*, 11556–11559.
- [74] P. Chen, H. Chen, J. Qiu, C. Zhou, *Nano Res.* **2010**, *3*, 594–600.
- [75] L. Zheng, Y. Xu, D. Jin, Y. Xie, *J. Mater. Chem.* **2010**, *20*, 7135–7143.
- [76] H. Song, J. Fu, K. Ding, C. Huang, K. Wu, X. Zhang, B. Gao, K. Huo, X. Peng, P. K. Chu, *J. Power Sources* **2016**, *328*, 599–606.
- [77] X. Zhao, C. Johnston, A. Crossley, P. S. Granta, *J. Mater. Chem.* **2010**, *20*, 7637–7644.
- [78] X. Xia, J. Tu, Y. Mai, X. Wang, C. Gu, X. Zhao, *J. Mater. Chem.* **2011**, *21*, 9319–9325.
- [79] X. Sheng, D. He, J. Yang, K. Zhu, X. Feng, *Nano Lett.* **2014**, *14*, 1848–1852.
- [80] Y. Liu, Y. Jiao, Z. Zhang, F. Qu, A. Umar, Xiang Wu, *ACS Appl. Mater. Interfaces* **2014**, *6*, 2174–2184.
- [81] X. Lu, G. Wang, T. Zhai, M. Yu, S. Xie, Y. Ling, C. Liang, Y. Tong, Y. Li, *Nano Lett.* **2012**, *12*, 5376–5381.
- [82] J. Jiang, J. Liu, R. Ding, X. Ji, Y. Hu, X. Li, A. Hu, F. Wu, Z. Zhu, X. Huang, *J. Phys. Chem. C* **2010**, *114*, 929–932.
- [83] S. Maiti, A. Pramanik, S. Mahanty, *ACS Appl. Mater. Interfaces* **2014**, *6*, 10754–10762.
- [84] L. Yuan, X.-H. Lu, X. Xiao, T. Zhai, J. Dai, F. Zhang, B. Hu, X. Wang, L. Gong, J. Chen, C. Hu, Y. Tong, J. Zhou, Z. L. Wang, *ACS Nano* **2012**, *6*, 656–661.
- [85] H. Xia, J. Feng, H. Wang, M. O. Lai, L. Lu, *J. Power Sources* **2010**, *195*, 4410–4413.
- [86] M.-S. Wu, Z.-S. Guo, J.-J. Jow, *J. Phys. Chem. C* **2010**, *114*, 21861–21867.
- [87] P. Yang, Y. Li, Z. Lin, Y. Ding, S. Yue, C. P. Wong, X. Cai, S. Tan, W. Mai, *J. Mater. Chem. A* **2014**, *2*, 595–599.
- [88] W. Liu, X. Yan, J. Chen, Y. Feng, Q. Xue, *Nanoscale* **2013**, *5*, 6053–6062.

- [89] H. R. Ghenaatiana, M. F. Mousavia, M. S. Rahmanifar, *Electrochim. Acta* **2012**, *78*, 212–222.
- [90] R. Liu, S. I. Cho, S. B. Lee, *Nanotechnology* **2008**, *19*, 215710.
- [91] J. Luo, Z. Zheng, A. Kumamoto, W. I. Unah, S. Yan, Y. H. Ikuhara, X. Xiang, X. Zu, W. Zhou, *Chem. Commun.* **2018**, *54*, 794–797.
- [92] S. Cavaliere, S. Subianto, I. Savych, D. J. Jones, J. Roziere, *Energy Environ. Sci.* **2011**, *4*, 4761–4785.
- [93] X. Li, Y. Chen, H. Huang, Y.-W. Mai, L. Zhou, *Energy Storage Mater.* **2016**, *5*, 58–92.
- [94] Y. Bian, R. Wang, S. Wang, C. Yao, W. Ren, C. Chen, L. Zhang, *J. Mater. Chem. A* **2018**, *6*, 15807–15814.
- [95] Y.-E. Zhu, L. Yang, J. Sheng, Y. Chen, H. Gu, J. Wei, Z. Zhou, *Adv. Energy Mater.* **2017**, *7*, 1701222.
- [96] G. Zhang, X. Xiao, B. Li, P. Gu, H. Xue, H. Pang, *J. Mater. Chem. A* **2017**, *5*, 8155–8186.
- [97] W. Lu, L. W. Liang, X. Sun, X. F. Sun, C. Wu, L. R. Hou, J. F. Sun, C. Z. Yuan, *Nanomaterials* **2017**, *7*, 325.
- [98] Q. Ren, Y. Zhang, H. Lu, Y. Wang, W. Liu, X. Ji, A. Devi, A. Jiang, D. W. Zhang, *ACS Appl. Mater. Interfaces* **2018**, *10*, 468–476.
- [99] W. Yan, J. Y. Kim, W. Xing, K. C. Donavan, T. Ayvazian, R. M. Penner, *Chem. Mater.* **2012**, *24*, 2382–2390.
- [100] H. Hua, S. J. Liu, Z. Y. Chen, R. Q. Bao, Y. Y. Shi, L. R. Hou, G. Pang, K. N. Hui, X. G. Zhang, C. Z. Yuan, *Sci. Rep.* **2016**, *6*, 20973.
- [101] K. Zhou, Y. He, Q. Xu, Q. Zhang, A. Zhou, Z. Lu, L.-K. Yang, Y. Jiang, D. Ge, X. Y. Liu, H. Bai, *ACS Nano* **2018**, *12*, 5888–5894.
- [102] Y.-E Miao, W. Fan, D. Chen, T. Liu, *ACS Appl. Mater. Interfaces* **2013**, *5*, 4423–4428.
- [103] H. Zhou, Y. Zhang, *J. Phys. Chem. C* **2014**, *118*, 5626–5636.
- [104] D. Sarkar, M. Mandal, K. Mandal, *ACS Appl. Mater. Interfaces* **2013**, *5*, 11995–12004.
- [105] W. Li, K. Xu, L. An, F. Jiang, X. Zhou, J. Yang, Z. Chen, R. Zou, J. Hu, *J. Mater. Chem. A* **2014**, *2*, 1443–1447.
- [106] X. Meng, D. Deng, *J. Mater. Chem. A* **2016**, *4*, 6919–6925.
- [107] Z. Lv, Y. Luo, Y. Tang, J. Wei, Z. Zhu, X. Zhou, W. Li, Y. Zeng, W. Zhang, Y. Zhang, D. Qi, S. Pan, X. J. Loh, X. Chen, *Adv. Mater.* **2017**, *29*, 1704531.
- [108] G. Wang, X. Lu, Y. Ling, T. Zhai, H. Wang, Y. Tong, Y. Li, *ACS Nano* **2012**, *6*, 10296–10302.
- [109] G. Cheng, T. Kou, J. Zhang, C. Si, H. Gao, Z. Zhang, *Nano Energy* **2017**, *38*, 155–166.
- [110] W. Yan, T. Ayvazian, J. Kim, Y. Liu, K. C. Donavan, W. Xing, Y. Yang, J. C. Hemminger, R. M. Penner, *ACS Nano* **2011**, *5*, 8275–8287.
- [111] C. Z. Yuan, J. Y. Li, L. R. Hou, L. Yang, L. F. Shen, X. G. Zhang, *J. Mater. Chem.* **2012**, *22*, 16084–16090.
- [112] R. Peng, N. Wu, Y. Zheng, Y. Huang, Y. Luo, P. Yu, L. Zhuang, *ACS Appl. Mater. Interfaces* **2016**, *8*, 8474–8480.
- [113] X. Lu, M. Yu, T. Zhai, G. Wang, S. Xie, T. Liu, C. Liang, Y. Tong, Y. Li, *Nano Lett.* **2013**, *13*, 2628–2633.
- [114] X. Chen, M. Cheng, D. Chen, R. Wang, *ACS Appl. Mater. Interfaces* **2016**, *8*, 3892–3900.
- [115] L. R. Hou, L. Lian, D. K. Li, J. D. Lin, G. Pan, L. H. Zhang, X. G. Zhang, Q. A. Zhang, C. Z. Yuan, *RSC Adv.* **2013**, *3*, 21558–21562.
- [116] J. Zhu, W. Shi, N. Xiao, X. Rui, H. Tan, X. Lu, H. H. Hng, J. Ma, Q. Yan, *ACS Appl. Mater. Interfaces* **2012**, *4*, 2769–2774.
- [117] F. Zheng, G. Li, Y. Ou, Z. Wang, C. Su, Y. Tong, *Chem. Commun.* **2010**, *46*, 5021–5023.
- [118] W. Zhu, Z. Lu, G. Zhang, X. Lei, Z. Chang, J. Liu, X. Sun, *J. Mater. Chem. A* **2013**, *1*, 8327–8331.
- [119] L. Chen, Y. Zhou, H. Dai, T. Yu, J. Liu, Z. Zou, *Nano Energy* **2015**, *11*, 697–703.
- [120] L. Wang, H. Yang, X. Liu, R. Zeng, M. Li, Y. Huang, X. Hu, *Angew. Chem. Int. Ed.* **2017**, *56*, 1105–1110.
- [121] K. Wang, J. Huang, Z. Wei, *J. Phys. Chem. C* **2010**, *114*, 8062–8067.
- [122] J. Huang, K. Wang, Z. Wei, *J. Mater. Chem.* **2010**, *20*, 1117–1121.
- [123] D. V. Pham, R. A. Patil, C.-C. Yang, W.-C. Yeh, Y. Liou, Y.-R. Ma, *Nano Energy* **2018**, *47*, 105–114.
- [124] X. Lu, Y. Zeng, M. Yu, T. Zhai, C. Liang, S. Xie, M.-S. Balogun, Y. Tong, *Adv. Mater.* **2014**, *26*, 3148–3155.
- [125] R. B. Rakhi, W. Chen, D. Cha, H. N. Alshareef, *Nano Lett.* **2012**, *12*, 2559–2567.
- [126] X. Lu, G. Wang, T. Zhai, M. Yu, J. Gan, Y. Tong, Y. Li, *Nano Lett.* **2012**, *12*, 1690–1696.
- [127] M. Yu, Y. Han, X. Cheng, L. Hu, Y. Zeng, M. Chen, F. Cheng, X. Lu, Y. Tong, *Adv. Mater.* **2015**, *27*, 3085–3091.
- [128] B. K. Deka, A. Hazarika, J. Kima, N. Kimb, H. E. Jeonga, Y.-B. Parka, H. W. Park, *Chem. Eng. J.* **2019**, *355*, 551–559.
- [129] H. Wu, Z. Lou, H. Yang, G. Shen, *Nanoscale* **2015**, *7*, 1921–1926.
- [130] Y. Chen, B. Liu, Q. Liu, J. Wang, Z. Li, X. Jing, L. Liu, *Nanoscale* **2015**, *7*, 15159–15167.
- [131] A. M. Elshahawy, X. Li, H. Zhang, Y. Hu, K. H. Ho, C. Guan, J. Wang, *J. Mater. Chem. A* **2017**, *5*, 7494–7506.
- [132] C. Z. Yuan, B. Gao, L. F. Shen, S. D. Yang, L. Hao, X. J. Lu, F. Zhang, L. J. Zhang, X. G. Zhang, *Nanoscale* **2011**, *3*, 529–545.
- [133] S. Boukhalfa, K. Evanoff, G. Yushin, *Energy Environ. Sci.* **2012**, *5*, 6872–6879.
- [134] C. Z. Yuan, L. F. Shen, F. Zhang, X. J. Lu, D. K. Li, X. G. Zhang, *J. Colloid Interface Sci.* **2010**, *349*, 181–185.
- [135] L. Li, Z. A. Hu, N. An, Y. Y. Yang, Z. M. Li, H. Y. Wu, *J. Phys. Chem. C* **2014**, *118*, 22865–22872.
- [136] X. Zang, C. Shen, E. Kao, R. Warren, R. Zhang, K. S. Teh, J. Zhong, M. Wei, B. Li, Y. Chu, M. Sanghadasa, A. Schwartzberg, L. Lin, *Adv. Mater.* **2017**, *29*, 1704754.
- [137] C. Nan, Z. Lin, H. Liao, M.-K. Song, Y. Li, E. J. Cairns, *J. Am. Chem. Soc.* **2014**, *136*, 4659–4663.
- [138] S. Fang, Z. Tong, P. Nie, G. Liu, X. Zhang, *ACS Appl. Mater. Interfaces* **2017**, *9*, 18766–18773.
- [139] X. Cao, B. Zheng, W. Shi, J. Yang, Z. Fan, Z. Luo, X. Rui, B. Chen, Q. Yan, H. Zhang, *Adv. Mater.* **2015**, *27*, 4695–4701.
- [140] C. Zhou, Y. Zhang, Y. Li, J. Liu, *Nano Lett.* **2013**, *13*, 2078–2085.
- [141] G.-F. Chen, X.-X. Li, L.-Y. Zhang, N. Li, T. Y. Ma, Z.-Q. Liu, *Adv. Mater.* **2016**, *28*, 7680–7687.
- [142] X. He, Y. Zhao, R. Chen, H. Zhang, J. Liu, Q. Liu, D. Song, R. Li, J. Wang, *ACS Sustainable Chem. Eng.* **2018**, *6*, 14945–14954.
- [143] C. Li, Z. Wang, S. Li, J. Cheng, Y. Zhang, J. Zhou, D. Yang, D.-G. Tong, B. Wang, *ACS Appl. Mater. Interfaces* **2018**, *10*, 18390–18399.
- [144] D. Kong, W. Ren, C. Cheng, Y. Wang, Z. Huang, H. Y. Yang, *ACS Appl. Mater. Interfaces* **2015**, *7*, 21334–21346.
- [145] L. Ren, G. Zhang, Z. Yan, L. Kang, H. Xu, F. Shi, Z. Lei, Z.-H. Liu, *ACS Appl. Mater. Interfaces* **2015**, *7*, 28294–28302.
- [146] P. Man, Q. Zhang, J. Sun, J. Guo, X. Wang, Z. Zhou, B. He, Q. Li, L. Xie, J. Zhao, C. Li, Q. Li, Y. Yao, *Carbon* **2018**, *139*, 21–28.
- [147] J. Rodriguez-Moreno, E. Navarrete-Astorga, E. A. Dalchiele, R. Schreiber, J. Ramos-Barrado, F. Martin, *Chem. Commun.* **2014**, *50*, 5652–5655.
- [148] J. Liu, J. Jiang, C. Cheng, H. Li, J. Zhang, H. Gong, H. J. Fan, *Adv. Mater.* **2011**, *23*, 2076–2081.
- [149] Q. Li, Z.-L. Wang, G.-R. Li, R. Guo, L.-X. Ding, Y.-X. Tong, *Nano Lett.* **2012**, *12*, 3803–3807.
- [150] L. Bao, J. Zang, X. Li, *Nano Lett.* **2011**, *11*, 1215–1220.
- [151] X. Lu, M. Yu, G. Wang, T. Zhai, S. Xie, Y. Ling, Y. Tong, Y. Li, *Adv. Mater.* **2013**, *25*, 267–272.
- [152] J. Wang, D. Chao, J. Liu, L. Li, L. Lai, J. Lin, Z. Shen, *Nano Energy* **2014**, *7*, 151–160.
- [153] W. Tian, X. Wang, C. Zhi, T. Zhai, D. Liu, C. Zhang, D. Golberg, Y. Bando, *Nano Energy* **2013**, *2*, 754–763.
- [154] G. Zhang, T. Wang, X. Yu, H. Zhang, H. Duan, B. Lu, *Nano Energy* **2013**, *2*, 586–594.
- [155] Y. Ai, X. Geng, Z. Lou, Z. M. Wang, G. Shen, *ACS Appl. Mater. Interfaces* **2015**, *7*, 24204–24211.
- [156] L. Yu, G. Zhang, C. Yuan, X. W. (David) Lou, *Chem. Commun.* **2013**, *49*, 137–139.
- [157] N. Liu, J. Li, W. Ma, W. Liu, Y. Shi, J. Tao, X. Zhang, J. Su, L. Li, Y. Gao, *ACS Appl. Mater. Interfaces* **2014**, *6*, 13627–13634.
- [158] L. Wang, M. Huang, S. Chen, L. Kang, X. He, Z. Lei, F. Shi, H. Xu, Z.-H. Liu, *J. Mater. Chem. A* **2017**, *5*, 19107–19115.
- [159] Y. Jiang, Z. Wu, L. Jiang, Z. Pan, P. Yang, W. Tian, L. Hu, *Nanoscale* **2018**, *10*, 12003–12010.
- [160] X. Song, C. Huang, Y. Qin, H. Li, H. C. Chen, *J. Mater. Chem. A* **2018**, *6*, 16205–16212.
- [161] J. Sun, Q. Zhang, X. Wang, J. Zhao, J. Guo, Z. Zhou, J. Zhang, P. Man, J. Sun, Q. Li, Y. Yao, *J. Mater. Chem. A* **2017**, *5*, 21153–21160.
- [162] H. B. Wu, H. Pang, X. W. Lou, *Energy Environ. Sci.* **2013**, *6*, 3619–3626.
- [163] T. Wu, J. Y. Li, L. R. Hou, C. Z. Yuan, L. Yang, X. G. Zhang, *Electrochim. Acta* **2012**, *81*, 172–178.
- [164] C. Z. Yuan, X. G. Zhang, L. R. Hou, L. F. Shen, D. K. Li, F. Zhang, C. G. Fan, J. M. Li, *J. Mater. Chem.* **2010**, *20*, 10809–10816.
- [165] C. Z. Yuan, J. Y. Li, L. R. Hou, J. D. Lin, X. G. Zhang, *J. Mater. Chem. A* **2013**, *1*, 11145–11151.
- [166] S. Ye, J. Feng, *ACS Appl. Mater. Interfaces* **2014**, *6*, 9671–9679.

- [167] R. Wang, J. Lang, P. Zhang, Z. Lin, X. Yan, *Adv. Funct. Mater.* **2015**, *25*, 2270–2278.
- [168] H. Huang, D. Kundu, R. Yan, E. Tervoort, X. Chen, L. Pan, M. Oschatz, M. Antonietti, M. Niederberger, *Adv. Energy Mater.* **2018**, *8*, 1802800.
- [169] S. Yang, Y. Liu, Y. Hao, X. Yang, W. A. Goddard III, X. L. Zhang, B. Cao, *Adv. Sci.* **2018**, *5*, 1700659.
- [170] M. T. Greiner, L. Chai, M. G. Helander, W.-M. Tang, Z.-H. Lu, *Adv. Funct. Mater.* **2012**, *22*, 4557.
- [171] H.-S. Kim, J. B. Cook, H. Lin, J. S. Ko, S. H. Tolbert, V. Ozolins, B. Dunn, *Nat. Mater.* **2017**, *16*, 454.
- [172] Y. Wang, T. Zhou, K. Jiang, P. Da, Z. Peng, J. Tang, B. Kong, W.-B. Cai, Z. Yang, G. Zheng, *Adv. Energy Mater.* **2014**, *4*, 1400696.
- [173] T. Zhai, S. Xie, M. Yu, P. Fang, C. Liang, X. Lu, Y. Tong, *Nano Energy*, **2014**, *8*, 255–263.
- [174] Y. Zeng, Y. Han, Y. Zhao, Y. Zeng, M. Yu, Y. Liu, H. Tang, Y. Tong, X. Lu, *Adv. Energy Mater.* **2015**, *5*, 1402176.
- [175] T. Zhai, X. Lu, Y. Ling, M. Yu, G. Wang, T. Liu, C. Liang, Y. Tong, Y. Li *Adv. Mater.* **2014**, *26*, 5869.
- [176] M. S. Javed, S. Dai, M. Wang, Y. Xi, Q. Lang, D. Guo, C. Hu, *Nanoscale* **2015**, *7*, 13610–13618.
- [177] V. Kumar, X. Wang, P. S. Lee, *Nanoscale* **2015**, *7*, 11777–11786.
- [178] Z. Li, J. Han, L. Fan, M. Wang, S. Tao, R. Guo, *Chem. Commun.* **2015**, *51*, 3053–3056.
- [179] X. Xia, Y. Zhang, D. Chao, Q. Xiong, Z. Fan, X. Tong, J. Tu, H. Zhang, H. J. Fan, *Energy Environ. Sci.* **2015**, *8*, 1559–1568.
- [180] G. Q. Zhang, H. B. Wu, H. E. Hostetler, M. B. Chan-Park, X. W. Lou, *Energy Environ. Sci.* **2012**, *5*, 9453–9456.
- [181] F. Grote, H. Zhao, Y. Lei, *J. Mater. Chem. A* **2015**, *3*, 3465–3470.
- [182] F.-X. Ma, L. Yu, C.-Y. Xu, X. W. (David) Lou, *Energy Environ. Sci.* **2016**, *9*, 862–866.
- [183] L.-F. Chen, Z.-Y. Yu, J.-J. Wang, Q.-X. Li, Z.-Q. Tan, Y.-W. Zhu, S.-H. Yu, *Nano Energy* **2015**, *11*, 119–128.
- [184] F. Zhang, C. Z. Yuan, X. J. Lu, L. Zhang, Q. Che, X. G. Zhang, *J. Power Sources* **2012**, *203*, 250–256.
- [185] M. Sathiya, A. S. Prakash, K. Ramesha, J.-M. Tarascon, A. K. Shukla, *J. Am. Chem. Soc.* **2011**, *133*, 16291–16299.
- [186] J. Wu, P. Guo, R. Mi, X. Liu, H. Zhang, J. Mei, H. Liu, W.-M. Lau, L.-M. Liu, *J. Mater. Chem. A* **2015**, *3*, 15331–15338.
- [187] A. K. Singh, D. Sarkar, G. G. Khan, K. Mandal, *J. Mater. Chem. A* **2013**, *1*, 12759–12767.
- [188] W. Ma, H. Nan, Z. Gu, B. Geng, X. Zhang, *J. Mater. Chem. A* **2015**, *3*, 5442–5448.
- [189] Y.-B. He, G.-R. Li, Z.-L. Wang, C.-Y. Su, Y.-X. Tong, *Energy Environ. Sci.* **2011**, *4*, 1288–1292.
- [190] X. Xia, J. Tu, Y. Zhang, X. Wang, C. Gu, X. Zhao, H. J. Fan, *ACS Nano* **2012**, *6*, 5531–5538.
- [191] C. Wei, H. Pang, B. Zhang, Q. Lu, S. Liang, F. Gao, *Sci. Rep.* **2013**, *3*, 2193.
- [192] X. Xiao, X. Peng, H. Jin, T. Li, C. Zhang, B. Gao, B. Hu, K. Huo, J. Zhou, *Adv. Mater.* **2013**, *25*, 5091.
- [193] S. Zhu, H. Zhang, P. Chen, L.-H. Nie, C.-H. Li, S.-K. Li, *J. Mater. Chem. A* **2015**, *3*, 1540–1548.
- [194] L. H. Su, X. G. Zhang, C. H. Mi, B. Gao, Y. Liu, *Phys. Chem. Chem. Phys.* **2009**, *11*, 2195–2202.
- [195] L. H. Su, L. Y. Gong, Y. Zhao, *Phys. Chem. Chem. Phys.* **2014**, *16*, 681–684.
- [196] H. Yu, J. Wu, L. Fan, K. Xu, X. Zhang, Y. Lin, J. Lin, *Electrochim. Acta* **2011**, *56*, 6881–6886.
- [197] H. Yu, J. Wu, J. Lin, L. Fan, M. Huang, Y. Lin, Y. Li, F. Yu, Z. Qiu, *ChemPhysChem* **2013**, *14*, 394–399.

Manuscript received: February 10, 2019

Revised manuscript received: May 4, 2019

Accepted manuscript online: May 17, 2019

Version of record online: July 2, 2019